MORPHING RESCUE ROBOT DESIGN AND FINITE ELEMENT ANALYSIS

BY

WANRUI HE

A THESIS
SUBMITTED TO THE FACULTY OF

ALFRED UNIVERSITY

IN PARTIAL FULFILLMENT OF THE REQUIREMENTS
FOR THE DEGREE OF

MASTER OF SCIENCE

IN

MECHANICAL ENGINEERING

ALFRED, NEW YORK

MAY, 2018

MORPHING RESCUE ROBOT DESIGN AND FINITE ELEMENT ANALYSIS

BY

WANRUI HE

B.S. ALFRED UNIVERSITY (2016)

SIGNATURE OF AUTHOR_____

APPROVED BY_____

DR. SEONG-JIN LEE, ADVISOR

_____

DR. EHSAN GHOTBI, ADVISORY COMMITTEE

_____

DR. JOE ROSICZKOWSKI, ADVISORY COMMITTEE

_____

CHAIR, ORAL THESIS DEFENSE

ACCEPTED BY_____

ALASTAIR CORMACK, INTERIM DEAN
KAZUO INAMORI SCHOOL OF ENGINEERING

ACKNOWLEDGMENTS

I feel much indebted to many people who have instructed and favoured me in the course of writing this paper. First, I would like to express my heartfelt gratitude to my advisor, Dr. Seong-Jin Lee, for his warm-heart encouragement and most valuable advice, especially for his insightful comments and suggestions on the draft of this paper. Without his help, encouragement and guidance, I could not have completed this paper. My sincere thanks also go to my thesis committee members Dr. Joe Rosiczkowski and Dr. Ehsan Ghobti, their help and support always guided me in the whole process of writing. I also want to thank Dr. Timothy Cox in particular, he was huge help my paper, and helped me made the paper better in writting.

Last, but not least. I would like to express my thinks to my parents Mr. Xuejian He and Mrs. Jin Cheng, for their in valuable encouragement and spiritual support during my studies.

TABLE OF CONTENTS

LIST OF TABLES

Page

LIST OF FIGURES

Page

ABSTRACT

In recent years, occurrence of all kinds of disasters has aroused wide scale attention to security of human society. Along with advances in technology, robots have found wide applications in the field of rescue. Over the past decade, different kinds of rescue robots have been developed, which mainly fall into three categories, namely crawler rescue robots, deformable (polymorphic) rescue robots and bionic rescue robots. The three types of robots have their respective advantages and disadvantages. They can be applied to different post-disaster environments.

In this thesis, the main idea was to design a structure for the rescue robot, enabling it to work according to different post-disaster environments. The structural design allowes the rescue robot to change its body size based on different sizes of the environmental space after a disaster so that the rescue robot could work in different sizes of environmental space. The design put forward in this thesis is an advanced version of Hoberman Sphere. Hoberman Sphere is an isolinetic structure which can expand and compress to varied sizes. In view of the structure of Hoberman, SolidWorks was employed to design a compressible and expandable structure to implement rescue tasks within a narrow space. In order to verify the feasibility of this design, the model was printed by 3D technology. A connection problem was observed with the model after being assembled and printed. Then, the model was further modified. Next, deformation and strain on this design under the stress were tested. ANSYS was adopted and used for the finite element analysis of the transient structure. The analysis results suggests that the deformation suffered by the external structure was the minimum, while the deformation within was more significant, but non rupture or deviation was found.

I. INTRODUCTION

A. Background of Intelligent Rescue Robot

Robots have broad prospects for development, with todays' robots third generation of robots, featuring a variety of sensors and integrating various sensory information. Moreover, they are capable of effectively adapting to changing environments, owing to their adaptive and autonomous learning ability and heightened functions. Intelligent robots incorporate multiple technologies across different technological sectors. The key technologies mainly belong to the fields of multi-sensor information coupling technology, multi-sensor information fusion, navigation and positioning technology, path planning technology, robot vision technology, intelligent control technology, and human-machine interface technology. Multi-sensor information fusion refers to comprehensive multi-sensor data perception, which produces more reliable, more accurate, and complete information. Furthermore, multi-sensor information improves multi-sensor system integration and accurately reflects the characteristics of detected objects, eliminating information uncertainty and improving information reliability. Navigation and positioning technologies take into account local, real-time obstacle avoidance and global planning, because it is necessary to accurately know the current state and location of robots and obstacles in order to navigate, avoid obstacles, and plan paths. Optimal path planning is based on one or more optimization criteria. Robot vision technology includes image acquisition, processing and analysis, output, and display, with its core task being feature extraction, image segmentation and identification. Intelligent control technology deals with

improving robot speed and accuracy while human and machine interface technology is concerned with facilitating human-machine communication.

Modern robots can complete a wide variety of complex tasks, such as deep-sea exploration, combat, reconnaissance, intelligence gathering, rescue, and service in response to human instructions. In addition to being able to complete work independently, they can also cooperate with other robots to accomplish tasks together or under human guidance. This technology has a wide range of applications in various fields.

Recently, earthquakes, fires, floods, terrorism, armed conflict, anthrax, SARS, avian influenza, and radioactive substances have aroused widespread concern for human safety. Although most people are alert and responsive to catastrophes, when it comes to dealing with destructive disasters, there are insufficient levels of preparation, and many people still die as a result of unprofessional and untimely rescues. Robotics technology, rescue technology, and disaster science have been collaborating in the development of a disaster rescue robot, but this is a challenging new field of robotics research.

Robotics technology first began in battlefield reconnaissance and military clean-up. Prior to the 1980s, scientists began developing notions of using robots in disaster rescue work. The year 1995 was a milepost in the history of rescue robot technology, when research into the field garnered more attention following the large-scale earthquake in Kobe, Japan[1]. New technologies then developed, and robots grew diverse in classification and function.

Disaster relief can be divided into three stages: pre-disaster rescue, disaster rescue, and post-disaster rescue. Pre-disaster rescue refers to disaster prevention and elimination, personnel evacuation, and goods transfer. Disaster rescue is a class of rescue and remedial

work which takes place during fires, floods, poisonous gas incidents, and radioactive substance incidents. Post-disaster rescue refers to sudden and short-term disasters such as earthquakes and explosions, as well as the subsequent search and rescue work. There are no absolute boundaries between disaster stages, but there are two problems present at all rescue stages: environment complexity and dangers. Taking the urban environment as an example, urbanization and urban population density are becoming increasingly serious issues, with high-rise buildings, underground works, large commercial and trade offices, and cultural and recreational places all developing at a rapid pace. The increasing number of urban buildings makes search and rescue operations very complicated. In certain disasters, there is an inherent risk of explosion, especially when the disaster relates to flammable, explosive, or toxic gases. After an earthquake there is a strong risk of buildings collapsing, which prevents rescue personnel from conducting in-depth reconnaissance or rescue, and while people are eager to detect internal dangers at disaster sites, they dare not approach or enter these sites. In such events, rescue robots can greatly improve rescue efficiency while reducing casualties for rescue personnel, because they not only help staff perform rescue operations, but also replace staff in performing search and rescue missions. Hence, rescue robots are playing an increasingly important role in disaster rescue.

B. Requirements of Disaster Rescue Robots

1. Survival (Viability)

Rescue robot survival mainly depends on reliability, durability, and adaptability of robot ontologies. In the post-disaster environment, the dangers of toxic gas, venom, biochemical substances, radioactivity, and secondary collapse make robot capacity for environmental adaptation especially important. In terms of temperature, there may be high temperatures in the environment after the disaster, and so robots must be able to withstand these adverse conditions, which necessitate adequate materials in robotic construction. In environments where toxic gasses or liquids are present, robots must face corrosion by toxicity, so material choice and structure sealing should be considered. In the post-disaster environment, the dangers of the environment must be considered in relation to robot surface strength and line safety. In the rescue robot's energy supply, it is necessary to use both wired and wireless methods to ensure sufficient power and working time. Another requirement for rescue robot survival is that, in order to perform different rescues in distinct disaster areas, robot hardware and software platforms need to be designed with flexibility in mind. Two similar disasters will not cause the exact same levels of nature of damage, and a single disaster will not have consistent effects in the affected environment. Therefore, when rescue robots encounter different and changeable situations, they should have adaptive and predictive abilities. They need to be able to adapt to the environment, be fit for challenging tasks, and be intelligent enough to cope with disturbances caused by various unstable and uncertain factors.

2. Mobility

Disaster environments require robots to have high mobility. Because of environmental constraints, a robot's physical structure must be small enough to navigate the confined spaces of ruins and pipes. Also, it must be able to overcome obstacles in its path, its center of gravity cannot be too high, and it must not lose traction when it passes over obstacles. Nevertheless, robots must cross various vertical obstacles, so platform stability and self-adjustive ability are very important. Sometimes, robots get damaged in disaster situations because of the characteristics intrinsic to disaster sites, low system reliability, and failure, meaning that system hardware and software fault tolerance as well as fault handling capacity are very important. In addition, the post-disaster environment contains soft soil, which alongside muddy roads and fires caused water damage, to function robots must have high ground adaptability, and wheeled-type, crawler-type, and leg-type mobile mechanisms, tracks, wheels, and leg composite mobile mechanisms need to be adopted.

3. Perception Ability

For rescue robots, sensors are the most vulnerable components. There are three main sensory criteria: robot control, environment detection, and victim detection. In order for robot control function correctly and for the robot's position, speed, and internal system state need to be monitored. The system can adopt the traditional robot CCD camera, laser rangefinder, ultrasonic range finder, contact and proximity sensor, infrared sensor, and radar positioning sensor. Furthermore, environmental inspections are very important for the normal operation of rescue robots, while also improving work efficiency, saving energy and preventing accidents. Environmental testing includes air quality detection and

monitoring (for levels of oxygen, hydrogen sulfide, methane and carbon dioxide) as well as detection of temperature, humidity, and radioactivity. These all influence human judgement in rescue environments, and which rescue robots can detect more easily than rescue workers. Environmental testing also involves geological and topographical tests of the ground environment, for two reasons: the avoidance of the obvious threats and the avoidance of greater damage to the environment, which could bring about a second collapse. Moreover, the static and dynamic conditions shapes and characteristics of terrains are always different, meaning terrain detection is intrinsically more difficult. For victim detection, systems monitor for human bodies, clothing, footprints, voices, body temperatures, and body position to determine whether those trapped are alive as well as various personal details to help identify them. In certain cases, the same detection system can also be used to search for animals.

C. Rescue Robot Development

Over the past decade, the United States, Japan, and other western countries have done a great deal of work to advance the study of earthquakes, fires, and rescue robots. Different rescue robots possess different kinds of traction and movement, which can be divided into the following categories: crawler rescue robots, deformable (polymorphic) rescue robots, and bionic rescue robots.

1. Crawler Rescue Robots

The crawler robot was developed to meet the needs of military reconnaissance and dangerous object demolition. The rescue robot is based on the traditional wheeled mobile robot. Figure 1 shows the typical products of several well-known robotics companies. Because of their design, which inhibits their agility, they are not suitable for narrow spaces for rescuing survivors in the rubble of collapsed buildings.

(a)Urbot robot from SPAWAR (b) SOLEM robot from Foster-Miller (c)Minitrac robot from Inuktun

Figure 1: Variants of the crawler rescue robot from three well-known robotics companies.[21]

2. Deformable (Polymorphic) Rescue Robots

To access narrow spaces, robots need to be as small as possible, but search field size further limits robot size. In order to solve this contradiction, in recent years traction-capable rescue robots, based on the traditional crawler, have developed polymorphic rescue robot designs. Figure 2 shows the Packbot robot series produced by Irobot. The Packbot robot has a pair of fin-shaped forelimbs, which the robot uses to navigate rugged terrain or raise the perception platform for enhanced observation.

(a) Packbot robot from Irobot (b) Upright position (c) Normal position

Figure 2: Different positions of the Packbot robot.[21]

Figure 3 shows a Micro VGTV polymorphic rescue robot produced by Canadian Inuktun. This robot is capable of flexibly adjusting its shape and size in accordance with search channel size and range.

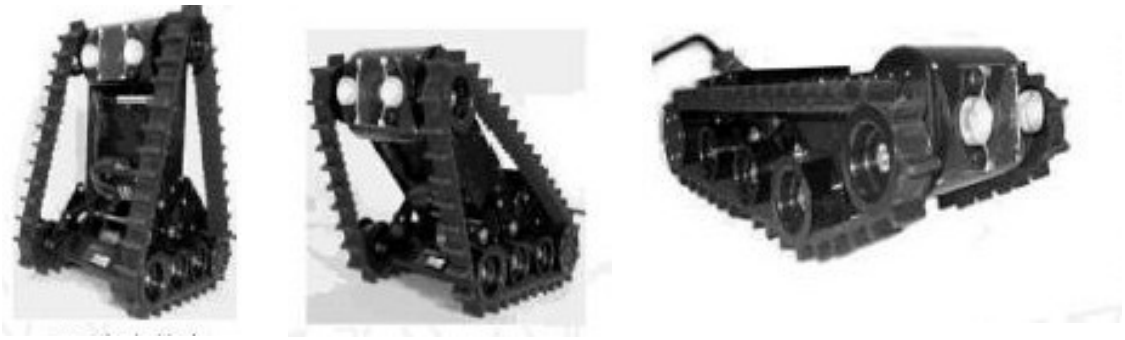

(a)Upright position (b) Semi-upright position (c) Normal position

Figure 3: Micro VGTV polymorphic rescue robots produced by Canadian Inuktun.[21]

3. Bionic Rescue Robots

Although tracked bionic robots can change shape and size in response to search space size, their volume is limited by driving mode restrictions. In order to meet search needs in narrow spaces, a host of bionic robots have been developed. These robots are smaller in volume thanks to ecological principles, namely, the mimicking of the natural motions of, among other animals, snakes. Figure 4(a) shows a fly rescue robot with a

height of less than 2cm, developed by the University of California. Figure 4(b) shows a snake robot developed by Osaka University. Figure 4(c) shows a mobile platform snake robot developed and installed by Carnegie Mellon University.

(a)A fly robot developed by University of California

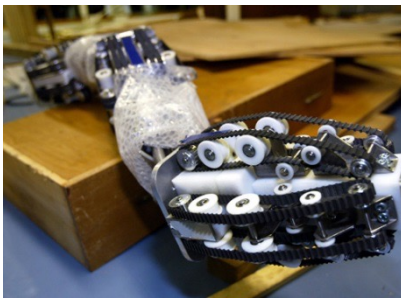

(b) Snake robot developed by Osaka University

(c) Mobile platform snake robot developed by CMU

Figure 4: Three bionic robots from different universities.[21]

D. Research Topic

Based on essential characteristics of all robots, this thesis referred to Hoberman Sphere's structure for the robot's basic appearance and structure design. Hoberman Sphere is an isolinetic structure which can expand and compress to varied sizes. The transformable structure of Hoberman Sphere could offer some reference for the design project in this paper. The essential characteristics found with most rescue robots were taken into consideration. The main purpose of the design project in this thesis was to allow a rescue robot to overcome obstacles in different spaces and environments so that the rescue robot could work in different rescue spaces and environments.

The robot designed in this thesis is for rescue, and provision of platform for investigation and checkout equipment, with the major character of simple structure. Its size can be changed and it is of strong obstacle climbing ability and can be easily controlled.

The structure's largest advantage is that rescue robot size can be changed based on deployable structure so that it is of good mobility and adaptability to environment. Moreover, its obstacle climbing ability is thus increased, so that its application is strengthened.

This thesis studies domestic and foreign rescue robot development status through learning movement theory of rescue robot, based on which, basic systematic structure of rescue robot is determined. Many space deployable structures have connected scissors-like unit as basic element. Further improvement of scissors-like unit and replacement of straight rod with folded rod will generate folded scissors-like unit whose angle can be adjusted, which is the basic element designed in the paper. Each scissors-like unit combination only has one degree of freedom in plane, which is thin and can easily lead to instability. Sufficient supporting plane should be considered to be designed. The design of space deployable structure is mainly to guarantee the unification of developability and stability, especially stability controllability in deployment. Finally, based on simple strength calculation of rescue robot structure, rescue robot structure was designed and structure was analyzed using finite elements.

Hoberman structure is a polygonal scissors structure. This kind of the structure has the advantage of being unfolded and folded to obtain a larger work face structure. The deployable structure can be easily transported and stored in a folded state, thus it can be used repeatedly. The Hoberman spherical structure can change the sphere size by changing its radius. The post-disaster environment is usually very complicated, while the deformable robot can make itself adaptable to surrounding environment according to different terrain environment requirements. This is why the Hoberman structure was chose the reference.

II. MODLING ANALYSIS AND LITEUREVIEW

A. Background of the Hoberman Sphere

The Hoberman sphere was created in 1990 by designer Chuck Hoberman, whose international career seamlessly fuses art, design, engineering, and architecture. Its unique approach has been most prominently showcased in the Hoberman Toy line, which was founded in 1995. Subsequent design explorations include rapidly deployable tents, miniature medical instruments, and juvenile products. [1] The Hoberman sphere is an isolinetic structure which can expand and compress to varied sizes. Figure 5 shows Hoberman Spheres fully expand and compressed.

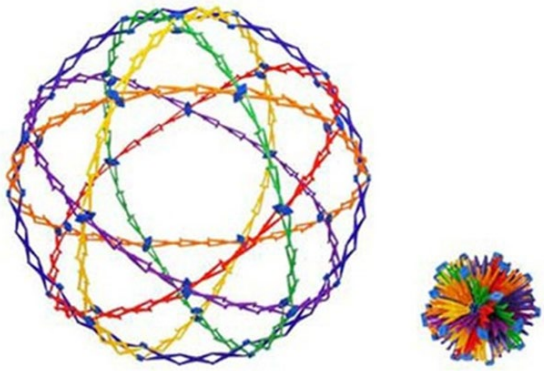

Figure 5: Hoberman Sphere expanded and collapsed (Hoberman Associates, Inc., 2014)[1]

Based on its structure, the robot is capable of increasing or decreasing its size to fit into different sized spaces. The robot can compress and expand to fit narrow spaces and carry out rescues. Figure 5 shows the toy based design of the Hoberman Sphere. It starts small and grows larger, and is made of rainbow-colored plastic links, meaning the sphere can expand to 30 inches in diameter and contracts to a compact 9.5 inches. Sarah Bolton, Dominic Doty and Peter Rivera (2014-2015) examined the compact deployable antenna

for CubeSat Units. They found that the Hoberman toy has a diameter ratio of 1.8 between the smaller and larger forms. Capability makes Hoberman Sphere robots an attractive scaffold, onto which an expandable antenna can be built. Moreover, as excessive joints reduce rigidity, reducing the number of joints can increase the collapsed diameter. [2]

The Hoberman Sphere is further considered a preferable concept design for its compactness, which is displayed in Figure 6. Like the AstroMesh, the Hoberman Sphere is a relatively lightweight design with small and thin subcomponents, and it boasts a large expansion ratio. However, this design requires a complex assembly of components in order to form the expanded arrangement of circular support rings. [2]

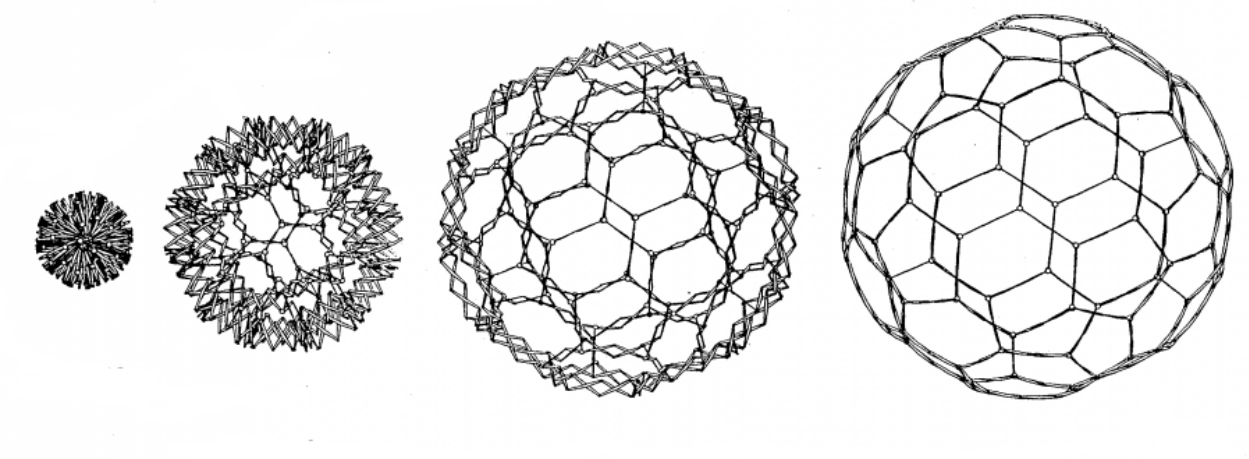

Figure 6: Schematic for the Hoberman Structure's expansion and contraction[2]

These high degree-of-freedom structures can be formed by a lattice of single degree-of-freedom polyhedral expanding units. Furthermore, with built-in symmetries, the entire structure can expand and contract in the same way as one of the units in the structure actuated by Sunil K. Agrawal, Saravana Kumar, Mark Yim and John W. Suh. Their thesis discussed the designs and workings of expanding spheres and expandagons, while also explaining how these mechanisms as a whole expand when one of the planar components

expands. Motivated by the Hoberman expanding structures, which use only prismatic joints instead of revolute joints, their thesis attempts to systematically describe a procedure for creating 3-dimensional expanding structures motivated by geometry of regular polyhedral shapes. Their thesis analyzes Hoberman structures to propose a new approach for designing and constructing single degree-of-freedom expanding structures using single degree-of-freedom expanding polyhedral units.[3] Figures 7 and 8 show designs based on a regular tetragon and hexagon. For Hoberman's designs, expanding spheres and expandagons incorporate revolute joints for the interconnecting components of the mechanism.

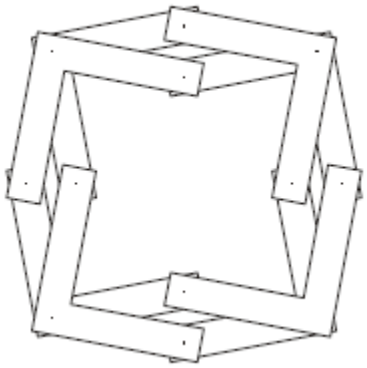

Figure 7: Schematic for an expanding tetragon based on Hoberman sphere design. [3]

Figure 8: Schematic for an expanding hexagon in the contracted and expanded states, based on
Hoberman sphere design. [3]

B. Hoberman structure

For this thesis, the structure design based on the Hoberman structure, before using the Hoberman structure, need to know how the structure works and what change can be made based on the structure. Analysis of Deployable Sturt Roof Structures deployable structures that can change shape form a compact to an expanded form by Maxwell H. Wolfe. In this thesis talked about angulated element structures in Chapter 5 which relayed to my research. To prove if the ends of the curved pantograph are connected to from a full circle, it will no longer be deployable, Figure 9 shows the single scissor-like element, made of two identical straight rods. To expand radially, the element must subtend a constant angle (α), and expand only along the lines OP and OR. [5]

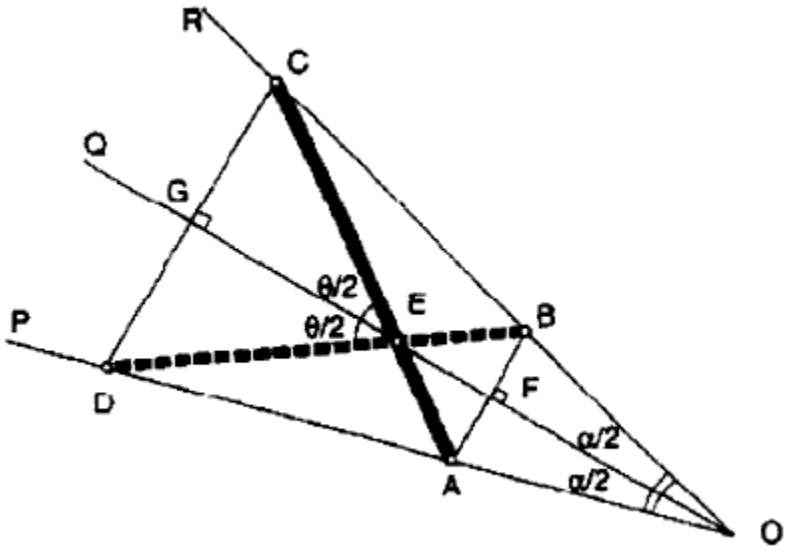

Figure 9: Off center pantograph made of straight, identical rods. [4]

From the Figure 9 note that CG and BF are proportional and the difference between the two is:

$$CG - BF = FG[\tan(\alpha/2)] \tag{1}$$

Expressing CG, BF and FG in terms of the deployment angle θ is:

$$CG = CE[\sin(\theta/2)] \tag{2}$$

$$BF = BE[\sin(\theta/2)] = AE[\sin(\theta/2)] \tag{3}$$

$$FG = AC[\cos(\theta/2)] \tag{4}$$

Though the equations about, and substituting yields and expression for α in term of θ:

$$\tan\left(\frac{\alpha}{2}\right) = \frac{CE - AE}{AC}[\tan(\frac{\theta}{2})] \tag{5}$$

Thus, alpha varies with the deployment angle and cannot remain constant during folding.[5] This means that a ring structure of straight pantographs cannot be deployed. To enable

movement, a kink the pantograph rods are introduced such that the center pivot is moved to a new point, as shown in Figure 10. The new equation relating alpha and theta is [5]:

$$\tan\left(\frac{\alpha}{2}\right) = \frac{CE - AE}{AC}\left[\tan\left(\frac{\theta}{2}\right)\right] + 2\left(\frac{EF}{AC}\right) \quad (6)$$

Therefore, if CE = AE, alpha is independent of theta and the structure can deploy as a mechanism. The angle of kink (also called the angle of embrace) in the angulated rod is $180^{o} - \alpha$.

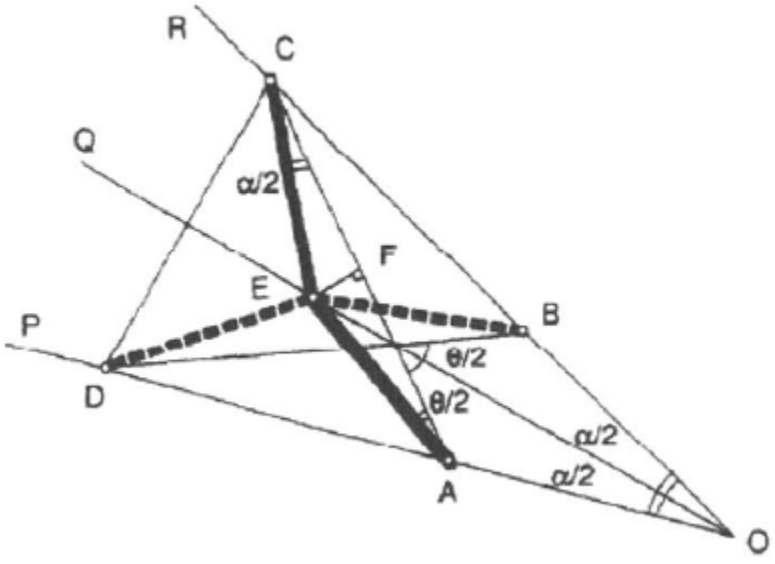

Figure 10: Kinked pantograph, or angulated element. [4]

According to the prove shown above, for my research, to use the angulated element create a circle by change angles of ∠AEC and ∠BED in Figure 10. The angulated elements of a general type can be creating as long as the triangles formed by ADE and BCE are isosceles or similar.

The Kinematic Theory for Radially Foldable Planar Linkages written by Jiten Patel and G.K. Ananthasuresh. This paper has proved to be versatile in giving a wide range of

2-D and 3-D foldable structures with a single degree of freedom. Figure 11 shows the planar foldable linkage by using Hoberman's structure, the highlights in Figure 11(a), (b) and (c) are the linkage that relied to angulated element which shows above in Figure 10.

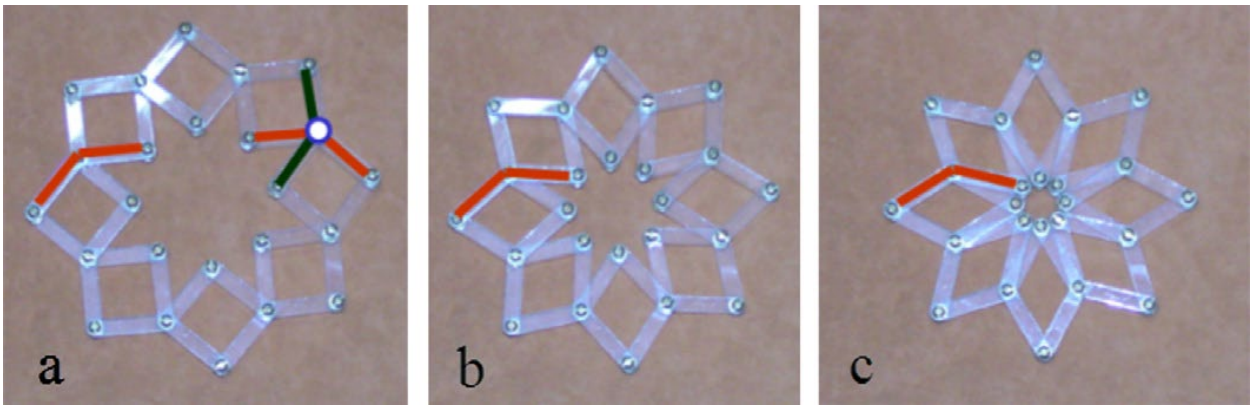

Figure 11: Hoberman's planar foldable linkage. The basic building block is shown using superimposed red angulated line in a–c. (a) also highlights the basic pair that folds. (For interpretation of the references to color in this figure legend, the reader is referred to the web
version of this article.)[6]

Figure 12(a) shows a pair of angulated elements of Hoberman's structure that enclose an angle at the center, since points A, C, D and E are constrained to move along of the dashed lines, so the two angulated elements as a pair of connected PRRP (prismatic-revolute-revolute-prismatic) linkages, and a PRRP linkage consists of two sliding (prismatic) joints and two hinge (revolute) joints. In the Hoberman's element, the coupler point of the PRRP is point B which shows in Figure 12(b). In Figure 12(c), it is a general pair of angulated elements (equivalently a pair of general PRRP linkages), from the Grubler's formula which gives zero degrees of freedom: $\{n = 7, j1 = 9, j2 = 0\} \Rightarrow 3(n - 1) - 2j_1 - j_2 = 0$. [6] The reason why $n = 7$, because there are two rigid triangles, four sliders and the fixed reference frame, $j_1 = 9$ because there are four sliding joints and five hinges.[6]

Though the Figure 8(a), (b) and (c), if the two pairs both share the same coupler curve at point B, then there will be movable.

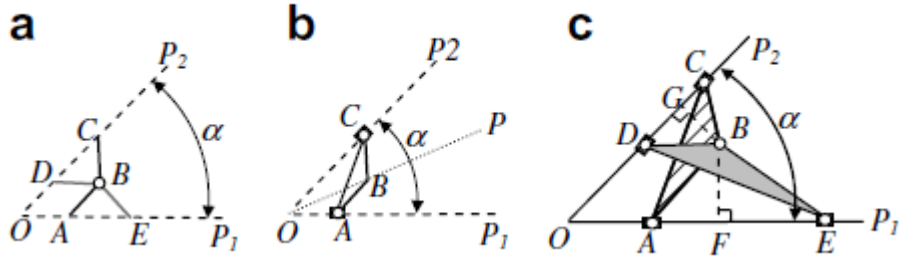

Figure 12: Kinematic interpretation of Hoberman's angulated element (a) a pair of Hoberman's angulated elements (b) a PRRP linkage interpretation of an angulated element (c) a pair of general PRRP linkages sharing a common coupler point B. [6]

On 1978, Hunt explanted the equation of the coupler curve of a PRRP planar four-bar linkage is a special sextic with many properties, and using the same procedure, the algebraic equation of the coupler curve of a PRRP linkage shows below.[7]

From Figure 13, by choosing the four geometric variables {p, q, ϕ, α} that define the linkage and another parameter γ that decides a particular configuration of the linkage, then the coordinates of points A, B and C will be written as[6]:

$$A: \{x - p(cos\gamma), y - p(sin\gamma)\} \tag{7}$$

$$B: \{x, y\} \tag{8}$$

$$C: \{x + qcos(\pi - \phi + \gamma), y + qsin(\pi - \phi + \gamma)\} \tag{9}$$

From the Figure 13 noting that the y-coordinate of point A is zero and the y-coordinate of C is divided by its x-coordinate tan (α), to solve the two equations for sin (γ) and cos (γ), thus :

$$\sin(\gamma) = \frac{y}{p} \tag{10}$$

$$\cos(\gamma) = \frac{(qcos(\phi) - qtan(\alpha)\sin(\phi) - p)y + (ptan(\alpha))x}{pq(\sin(\phi) + \tan(\alpha)\cos(\phi))} \tag{11}$$

At point B, the equation of the coupler curve can get by using the identity $\sin^2\gamma + \cos^2\gamma = 1$.

$$C_{x^2}x^2 + C_{y^2}y^2 + C_{xy}xy + C = 0 \tag{12}$$

Since:

$$C_{x^2} = p^2tan^2\alpha \tag{13}$$

$$C_{y^2} = q^2 + q^2tan^2\alpha + p^2 - 2pqcos(\phi) + 2pqtan(\alpha)\sin(\phi) \tag{14}$$

$$C_{xy} = -2pqtan^2(\alpha)\sin(\phi) + 2pqtan(\alpha)\cos(\phi) - 2p^2\tan(\alpha) \tag{15}$$

$$C = -p^2q^2(\tan(\alpha)\cos(\phi) + \sin(\phi))^2 \tag{16}$$

From the second degree polynomial equation and with g = f = 0, the equation yields:

$$ax^2 + by^2 + 2hxy + 2gx + 2fy + c = 0 \tag{17}$$

In the PRRP linkage, all four different values of {p, q, ϕ, α} will represent different geometric entities as summarized below:

$$(i)\ A\ pair\ of\ straight\ lines\ if\ \Delta = abc + 2fgh - af^2 - bg^2 - ch^2 = 0. \tag{18}$$

$$(ii)\ A\ parabola\ if\ h^2 - ab = 0\ and\ \Delta \neq 0. \tag{19}$$

$$(iii)\ A\ hyperbola\ if\ h^2 - ab > 0\ and\ \Delta \neq 0. \tag{20}$$

$$(iv)\ An\ ellipse\ if\ h^2 - ab < 0\ and\ \Delta \neq 0. \tag{21}$$

$$(v)\ A\ pair\ of\ parallel\ or\ coincidental\ lines\ if\ h^2 - ab = 0\ and\ \Delta = 0. \tag{22}$$

$$(vi)\ A\ circle\ if\ a = b\ and\ h = 0. \tag{23}$$

These six equations had shown how to derive linkages properties. For this thesis, the equations from 18 to 23 will be use, because Hoberman sphere is made based on circle structure, and the design of this thesis project which base on Hoberman sphere. So at this time, only the circle equation will be used on this thesis.

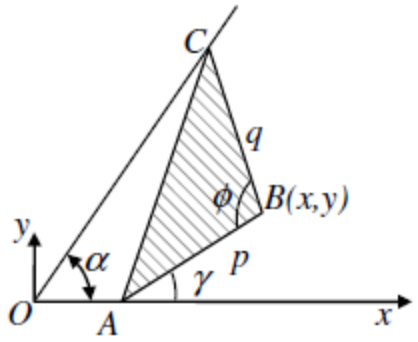

Figure 13: The schematic of a PRRP linkage and its coupler point, B. [6]

Hoberman's linkage is a special case of the PRRP. Hoberman's design is the two triangles in the PRRP linkage pair are identical and hence the triangles are congruent. So, when m = 1 implies that $p_1 = p_2 = q_1 = q_2$ in addition to $\phi_1 = \phi_2$. Then the result is [6]:

$$\tan(\alpha) = \frac{\phi_1(p_1 + q_1)}{p_1 q_1 - \phi_1^2} = \frac{2\phi_1 p_1}{p_1^2 - \phi_1^2} = \frac{2(\phi_1/p_1)}{1 - (\phi_1/p_1)^2} \tag{24}$$

$$\Longrightarrow \tan(2 * \alpha/2) = \frac{2\tan(tan^{-1}(\phi_1/p_1))}{1 - tan^2(tan^{-1}(\phi_1/p_1))} \tag{25}$$

$$\Longrightarrow \tan(\alpha/2) = (\phi_1/p_1) = (\phi_1/q_1) \tag{26}$$

The equation shown above is the condition of Hoberman's angulated element and the coupler curve of the Hoberman's angulated element is a radial straight line. When the

coupler curve becomes a circle, the circumferentially actuatable angulated element is possible.

III. EXPERIMENTAL PROCEDURE

As addressed in the Introduction, Hoberman structures, which are scissor structures, were used for deployable structure in this research.

The three vertices adjacent to the polygon P_{i-1}, P_i, P_{i+1}, made a scissor unit X_i, the lengths of the straight bars on the arms of a scissor unit's left and right sides are $b_i^{1,l} = b_i^{2,l} = \frac{\|P_{i-1}P_i\|}{2}$, $b_i^{1,r} = b_i^{2,r} = \frac{\|P_iP_{i+1}\|}{2}$, with the angle between the straight bars on both sides given as $\varphi_i^1 = \varphi_i^2 = \angle P_{i-1}P_iP_{i+1}$, and the connection point of two rigid arms as $o_{i,1} = o_{i,2} = P_i$. For adjacent two scissors units X_i and X_{i+1}, $b_i^{1,r} = b_i^{2,r} = b_{i+1}^{1,l} = b_{i+1}^{2,l} = \frac{\|P_iP_{i+1}\|}{2}$, which meant the quadrangle formed by two adjacent scissor units was diamond in shape (shows in Figure 14 (a)). For any one polygon, based on its two adjacent edges, n scissors units was constructed to fit the polygons.[13]

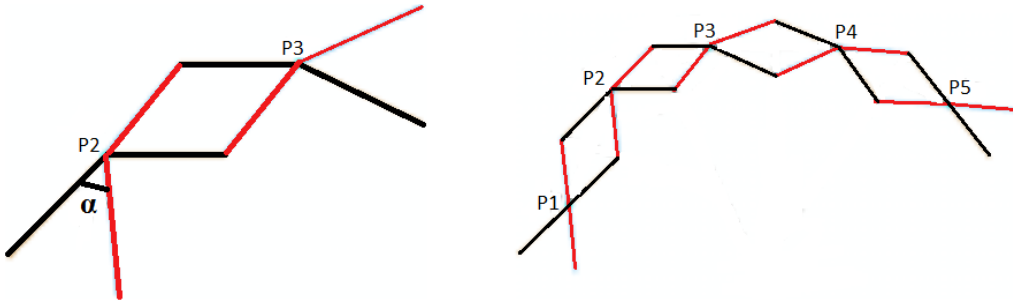

a. The connection of a scissors unit b. Partial polygonal scissor structure

Figure 14: Polygonal scissor structure

When calculating the changing rule of a side length (in Figure 14, $P_iP_{i+1,}i = 1, 2, 3, 4$) the isometric units need to be satisfied such that $\varphi^1 = \varphi^2$in consideration of $P_2P_{3,}$ meaning that for any scissor unit, the angle α is equal when the two arms are folded. Therefore, each diamond shape in Figure 14 (b) was the same.

After folding, the polygonal scissor structures still have $\angle P_1' P_2' P_3' = \varphi_2^1 = \varphi_2^2$, and the length of $P_2' P_3'$ is: $\|P_2' P_3'\| = b_2^{1,r} \cdot \cos\frac{\alpha}{2} + b_3^{1,l} \cdot \cos\frac{\alpha}{2} = \|P_2 P_3\| \cdot \cos\frac{\alpha}{2}$. According to the same theory, following transformation, any interior angle $\angle P_{i'}' P_i' P_{i^*}'$ with length $\|P_i' P_{i^*}'\|$, gives $\angle P_{i'}' P_i' P_{i^*}' = \varphi_i^1$, $\|P_i' P_{i^*}'\| = \|P_i P_{i^*}\| \cdot \cos\frac{\alpha}{2}$, and $i = 0, 1, 2, \cdots, n-1, i' = (i-1) mod\ n, i^* = (i+1) mod\ n$. Therefore, the interior angles remained unchanged in the folding process, and each side's stretching ratio was the same. Thus, for polygonal scissor structure formed of equiangular elements, the polygon enclosed by the connection points of the two arms' scissor units were the folding transformation represent a similar change. In defining the fold factor η, the degree of scissor structure folding was given by [13]:

$$\eta = \frac{\|P_i P_{i^*}\|}{\|P_i' P_{i^*}'\|} = \sec\frac{\alpha}{2} \tag{27}$$

When η=1, the scissor unit angle α=0, meaning that no folding occured when the scissor structures first begin to fold, but when α increased, $\sec\frac{\alpha}{2}$ also increased. Therefore, the angle α was used to describe the folding degree of the polygonal scissor structure.

A. SolidWorks model design

Before designing the overall model, all individual components in the model must first be designed, for the purposes of this thesis, the most important components were the linkages. Next, in order to design the linkage angle between two arms, draw a 8-sided polygon, an octagon. The formula to determine each of the octagon's inner angles is: $\theta =$

$\frac{(n-2)*180}{n}$, by using n = 8, we get θ = 135° . As shown in Figure 15, we have an octagon with a circle inside, so by increasing the number of sides of the outer polygon n, the polygon more closely resemble a circle. As shown in Figure 16, using n = 16 produces a hexakaidecagon, which means θ = 157.5°. Linkages are designed based on the angle θ. The size of the circle depends on the number of linkages, and increasing the number of linkages increased the circle's diameter. If the number of linkages increased, angle θ would be recalculated using the inner angle formula shown above.

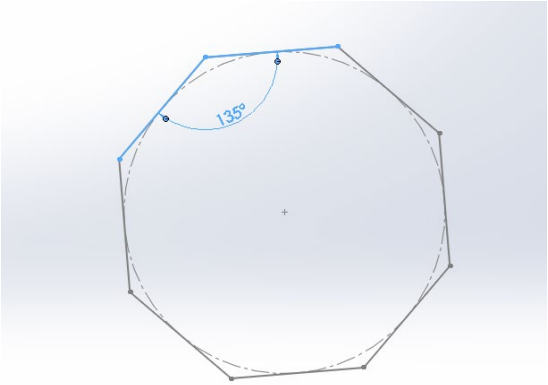

Figure 15: 2-D octagon with interior angle 135° in SolidWorks

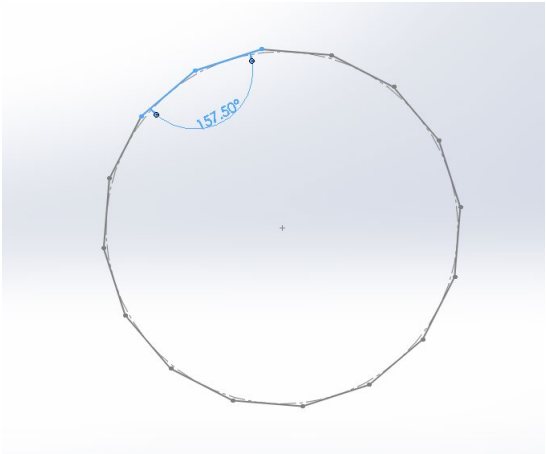

Figure 16: 2-D hexakaidecagon with interior angle 157.5° in SolidWorks

Based on the introduction, designing a pair of general prismatic-revolute-revolute-prismatic (PRRP) linkages required two different linkages, of the same shape but different sizes, to be designed. Figure 17 shows a three-dimensional model of one linkage for the general PRRP linkages in SolidWorks. This linkage has been named linkage-one. Figure 18 is a two-dimensional drawing of linkage-one in SolidWorks. Linkage-one has two different sides, with the left side 20 cm in length, the right side 24 cm, and the angle between the two 135^{o}. Linkage-one has three joint holes, each 2.5 cm in diameter. Moreover, the width of the right and left sides are 3.45 cm and 2.86 cm respectively, and linkage-one is 3.5 cm in thickness.

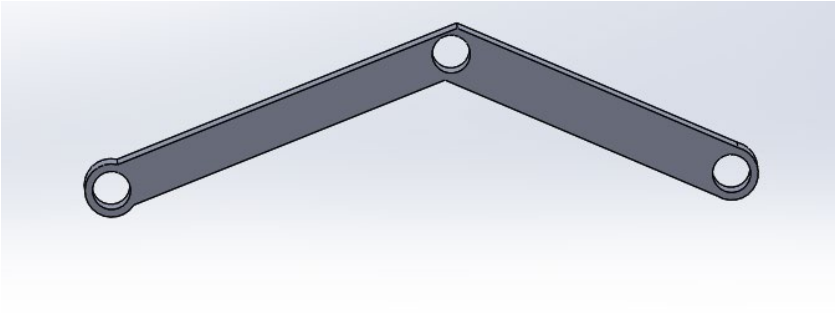

Figure 17: 3-D design of linkage-one in SolidWorks

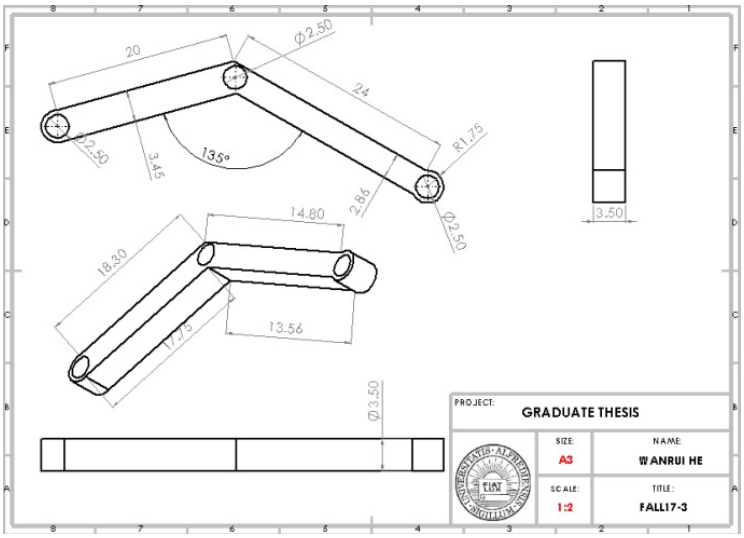

Figure 18: 2-D drawing of linkage-one in SolidWorks

Figure 19 shows a three-dimensional model of one linkage designed for the general PRRP linkages using SolidWorks. This linkage has been named linkage-two. Linkage-one and linkage-two are a pair of PRRP linkage that will later be used later to assemble the model. Figure 20 is a two-dimensional drawing of linkage-two in SolidWorks. Linkage-one has two different sides, with the left side 24 cm in length, the right side 20 cm, and the angle between the two 135º. Linkage-one has three joint holes, each 2.5 cm in diameter. The widths of the left and right sides are 3.45 cm and 2.86 cm respectively. Linkage-one is 3.5 cm thick in total.

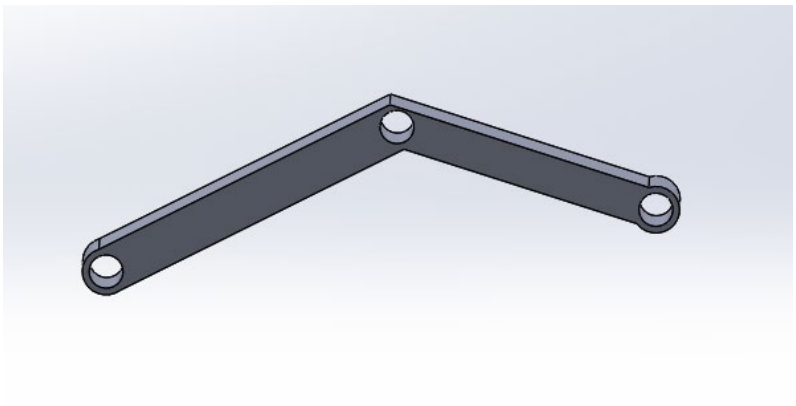

Figure 19: 3-D design of linkage-two in SolidWorks

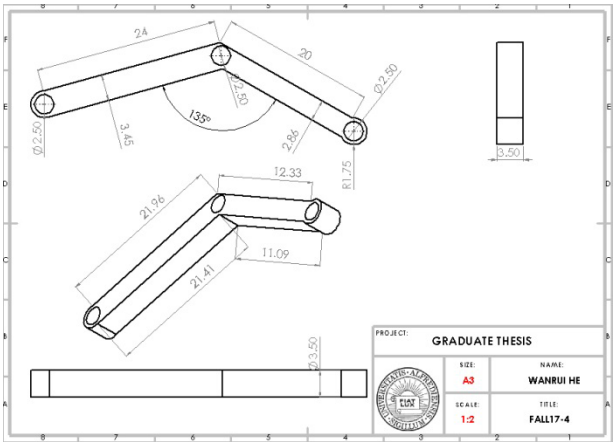

Figure 20: 2-D drawing of linkage-two in SolidWorks

Figure 21 shows a three-dimensional model of the connector designed in SolidWorks. This connector will later be used to assemble the model. Figure 22 is a two-dimensional drawing of the connector in SolidWorks. The connector is cross-planar with four holes. The four holes each have a diameter of 2.5 cm. The height and width of the connectors are 5 cm and 8 cm. Both planes are 0.5 cm thick.

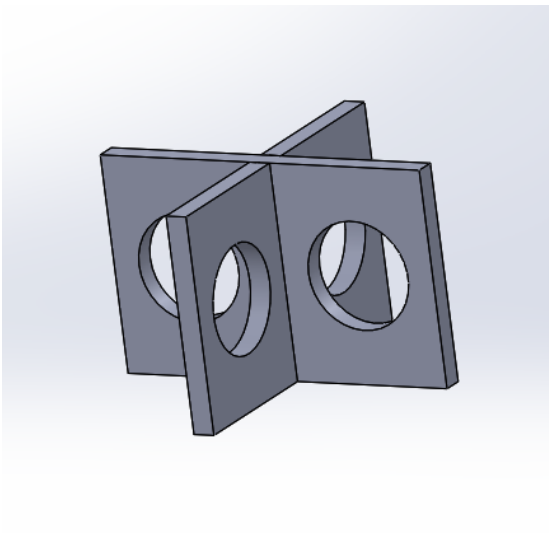

Figure 21: 3-D design of the connector in SolidWorks

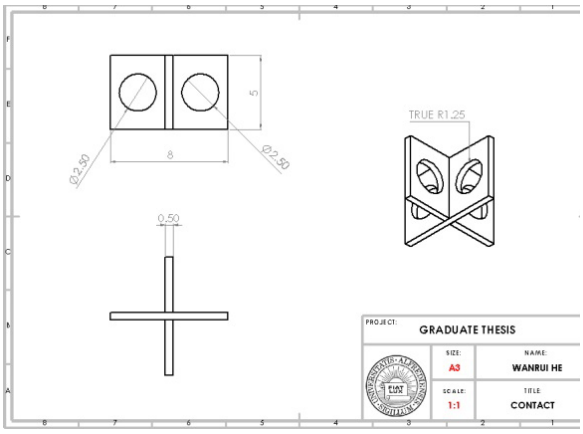

Figure 22: 2-D drawing of the connector in SolidWorks

Figure 23 shows a three-dimensional model of a pin designed in SolidWorks. This pin has been named a short pin and will later be used to assemble the model. Figure 24 is a two-dimensional drawing of a short pin in SolidWorks. A short pin is a cylinder 2.5 cm in diameter and 4 cm in length.

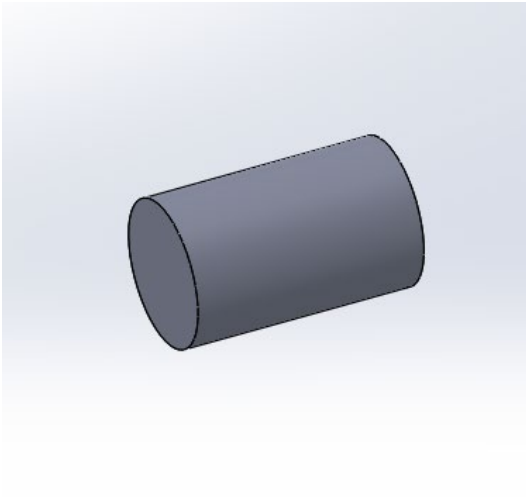

Figure 23: 3-D design of a short pin in SolidWorks

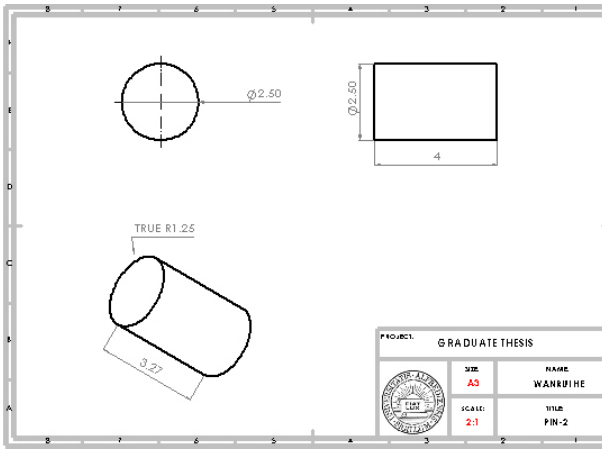

Figure 24: 2-D drawing of a short pin in SolidWorks

Figure 25 shows a three-dimensional model of a pin used to join two linkages together, designed in SolidWorks. This pin has been named a long pin and will later be used to assemble the model. Figure 26 is a two-dimensional drawing of a long pin in SolidWorks. A long pin is a cylinder 2.5 cm in diameter and 7.5 cm in length. Long and short pins are identical cylinders, differing only in length, because the two must connect different components.

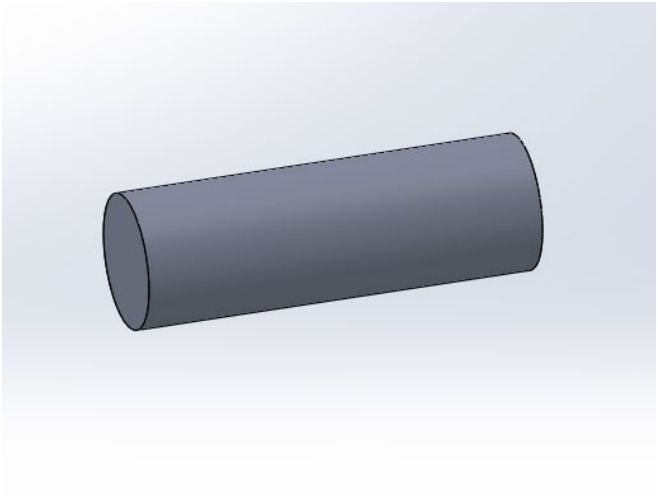

Figure 25: 3-D design of a long pin for linkages-one and linkages-two in SolidWorks

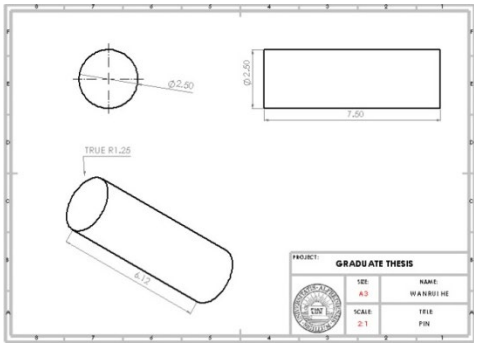

Figure 26: 2-D drawing of a long pin for linkages-one and linkages-two in SolidWorks

All components shown in Figure 17 through Figure 26 will be assembled to form the spherical structure shown in Figure 28. Figure 28 is a structure with three axes (x-axis, y-axis and z-axis), each of which will be assembled using eight linkages-one, eight linkages-two, eight connectors, sixteen short pins, and sixteen long pins. Figure 27 shows the structure of a single axis. As the sphere structure has three axes, three are required. The total components inventory for Figure 28 is twenty-four linkages-one, twenty-four linkages-two, twelve connectors, forty-eight short pins, and forty-eight long pins. The

reason only twelve connectors, rather than twenty-four, are needed is that any two axes share some connectors, hence, only twelve are required to form the sphere. When the structure expands, the sphere's diameter is 114.18 cm. Figure 29 is a two-dimensional drawing of the sphere structure in SolidWorks, this figure shows three different views of the structure.

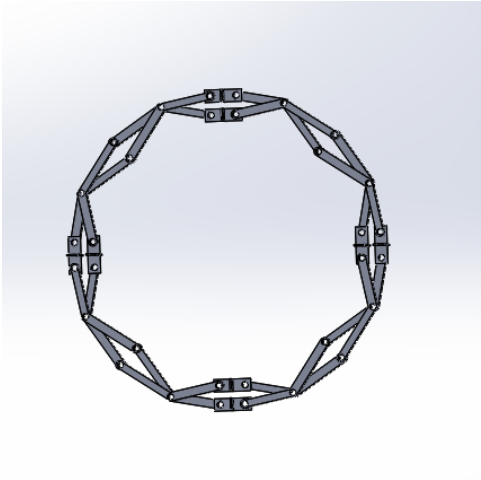

Figure 27: A single sphere axis

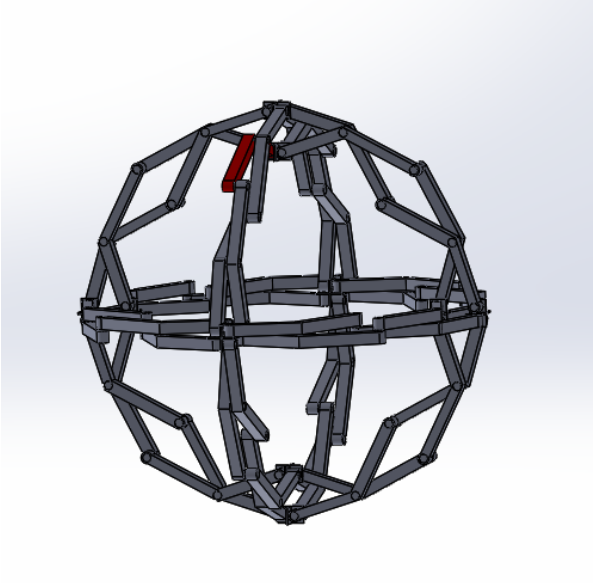

Figure 28: 3-D assembled model in SolidWorks

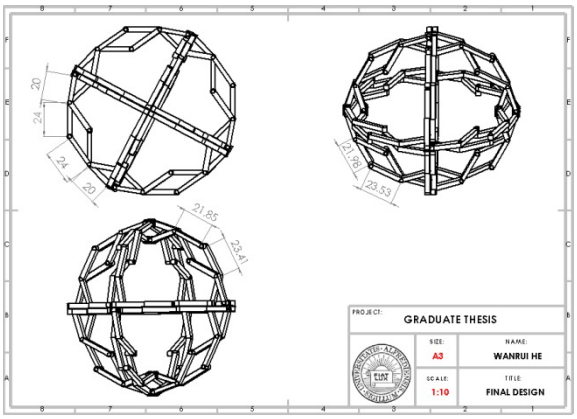

Figure 29: 2-D drawing of the assembled model in SolidWorks

Figure 30 showcases the connections between components. Linkages A, B, C and D are linkages-one and are assembled using pin 1, a long pin, in combination with linkages E, F, G and H, which are linkages-two, assembled in the same manner as linkage-one. Pin 2 is a short pin used to assemble the connectors.

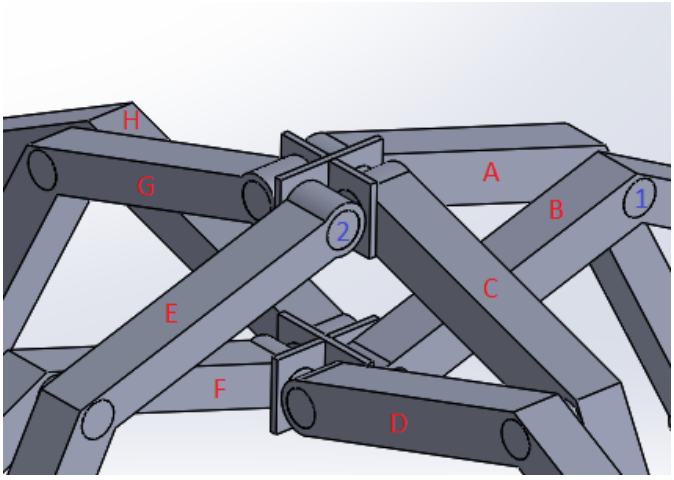

Figure 30: Detailed view of a connected point featuring all the linkages and pins in 3-D in SolidWorks

B. 3-D Printer Model

The easiest ways to test how the designed model works in real life is to 3-D print all the components and assemble the model. If the model works, then the designed model should work in real life. If there are any problems in the assembled model or assembly process, then it will be necessary to return to the SolidWorks model to resolve these problems. For this project, the 3-D printer used was a MakerBot Replicator Z18, the specifications of which are listed below:

Its operating dimensions: 305 × 305 × 457 mm

Positioning accuracy: XY-axis: 0.011 mm, Z-axis: 0.0025 mm

Print nozzle: Single nozzle

Nozzle diameter: 0.4 mm

Forming principle: Burning fiber

Material diameter: 1.75 mm (0.069'')

Material color: Gray

Figures 31 and 32 are 3-D prints of pairs of linkages-one and linkages-two, each connected by a long pin. Considering the size of the 3-D printer, all 3-D print components' sizes have been scaled down at a ratio of 3:1. All linkages exhibited zero problems during assembly.

Figure 31: 3-D print of a pair of linkages-one

Figure 32: 3-D print of a pair of linkages-two

After assembling the 3-D printed components, the structure is shown in Figures 33 and 34. Figure 33 is the contracted view of the assembly model, while Figure 34 is the expanded view. The 3-D assembly model is 1/3 the size of the SolidWorks model, because the printed model was scaled down to 33%. The assembled model can be expanded by pulling any two points. There were a few problems during assembly, with the biggest being the connectors. In Figure 14, A, C, E and G are shown connected by a single connector, while there were no problems in SolidWorks, during assembly, the connectors were not sufficiently thick, nor were the short pins long enough to stably connect the two. Hence, when assembling all the components, the twelve connectors were weak and easily broken. To resolve this, the connectors and short pins must be redesigned to ensure the structure is stable and moveable.

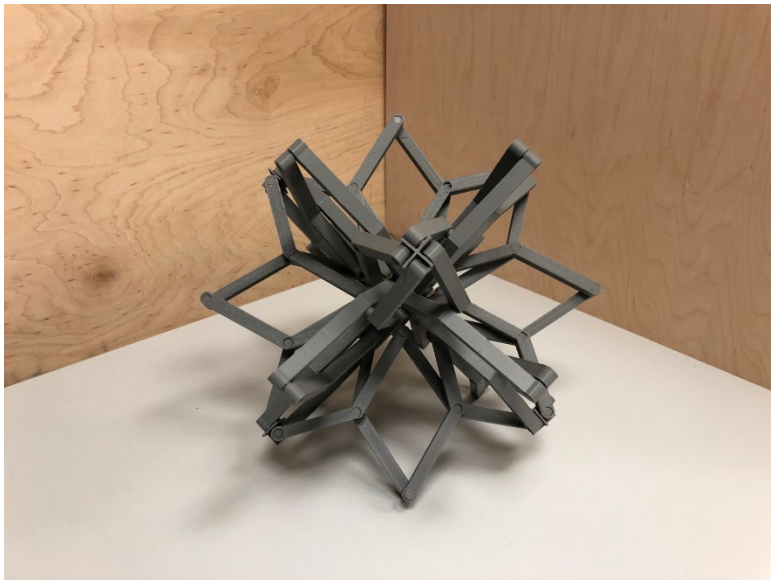

Figure 33: Contracted view of the 3-D printed assembly model

Figure 34: Expanded view of the 3-D printed assembly model

C. Second Version of Design model

To resolve the aforementioned problem, the components and model needed to be redesigned. The new model will be twice bigger than the previous model, with all linkages unchanged in shape and size, but with a different angle θ, and an increased amount of linkages. The reason for this increase is shown in Figure 16.

Figure 35 shows a redesigned three-dimensional model of linkage-one, redesigned based on the previous linkages in SolidWorks. This linkage has been named redesigned linkage-one. Figure 36 is a two-dimensional drawing of redesigned linkage-one in SolidWorks. Redesigned linkage-one has a left and right side, which are 20 cm and 24 cm in length respectively, just like the previous linkage-one, but with a new angle of 157.5 º. Redesigned linkage-one has three joint holes, each 2.5 cm in diameter. It's left and right sides are 3.45 cm and 2.86 cm in width respectively, and linkage-one is 3.5 cm thick. For

redesigned linkage-one, all variables are kept unchanged except for angle θ, which has changed from 135º to 157.5º.

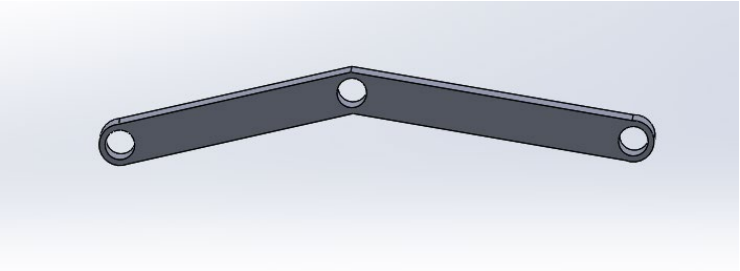

Figure 35: 3-D design of redesigned linkage-one in SolidWorks

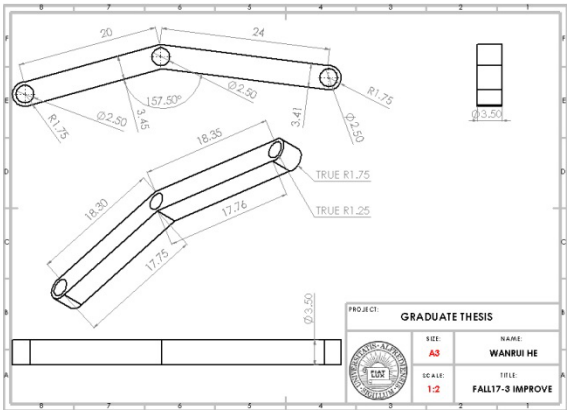

Figure 36: 2-D drawing of redesigned linkage-one in SolidWorks

Figure 37 shows a three-dimensional model of redesigned linkage-two, redesigned based on the previous linkages in SolidWorks. This linkage has been named redesigned linkage-two. Figure 38 is a two-dimensional drawing of redesigned linkage-two in SolidWorks. Redesigned linkage-two has a left and right side, which are 20 cm and 24 cm in length respectively, just like the previous linkage-two. Following the resigned, the angle between the two sides is now 157.5º. Redesigned linkage-two has three joint holes, each

2.5 cm in diameter. The widths of the left and right sides are 3.45 cm and 2.86 cm respectively. Redesigned linkage-two is 3.5 cm. For redesigned linkage-two, all variable are unchanged except for angle θ, which has changed from 135º to 157.5º.

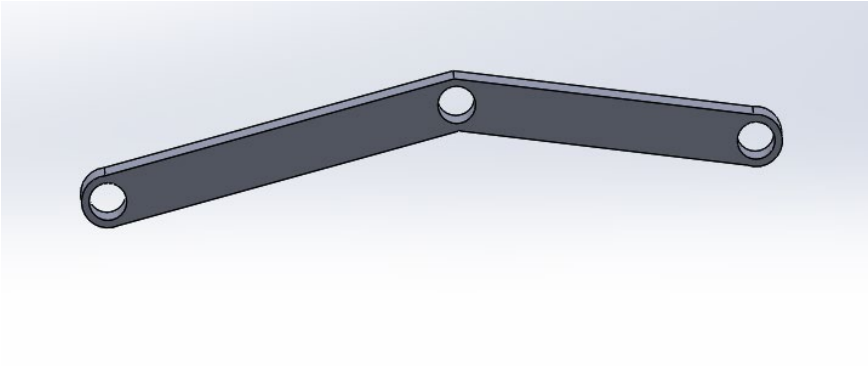

Figure 37: 3-D design of redesigned linkage-two in SolidWorks

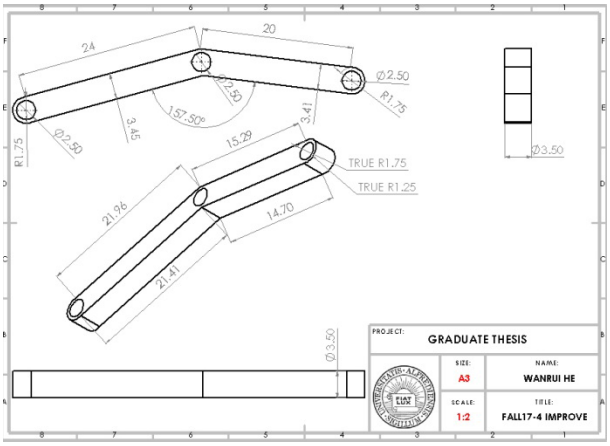

Figure 38: 2-D drawing of redesigned linkage-two in SolidWorks

In order to solve the connection problem of the previous model, the connector and a pin must be reimagined. Figure 39 shows a three-dimensional model of the redesigned connector. It was redesigned using SolidWorks. Figure 40 is a two-dimensional drawing of the redesigned connector in SolidWorks. The connector preserves the shape of the

previous one, and is a cross planar with four holes. The four holes each have the unchanged diameter of 2.5 cm. The height and width of the connectors are 5 cm and 15 cm respectively. The thickness of both planes is 0.5 cm. The only difference from the previous design is the width and height, with thickness and the holes remaining unchanged in size.

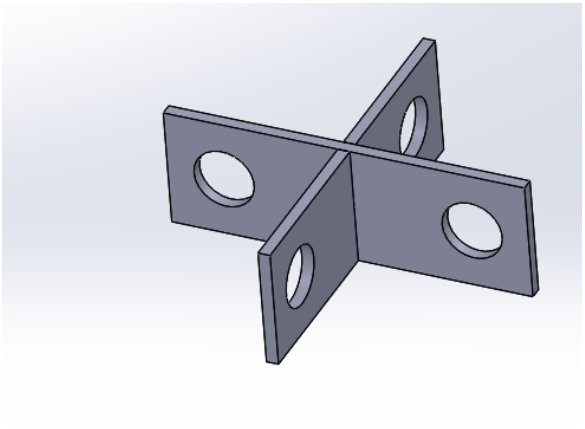

Figure 39: 3-D design of the resigned connector in SolidWorks

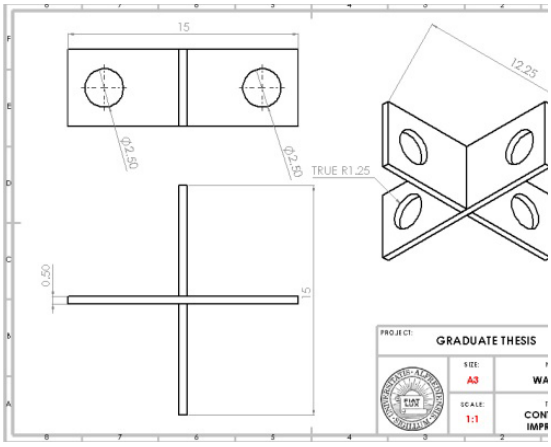

Figure 40: 2-D drawing of the redesigned connector component in SolidWorks

In redesigning the pins for the connectors and linkages, the most important factor to consider is structure mobility and stability. The best way to achieve this is to use a screw to connect the components, and any screw contains a bolt and nut. Figure 41 is the 3-D design of the bolt in SolidWorks. Because the bolt needs to connect the connector and yet be moveable, it cannot have all the thread. Thread should only be used to connect the nut, while the part without thread will connect with the connector. Figure 42 is a 2-D drawing of the bolt in SolidWorks, the total length of which is 7 cm. The head is 1cm, the none threaded shank 4 cm, the threaded shank 2 cm, and the threaded shank's diameter 2.1 cm.

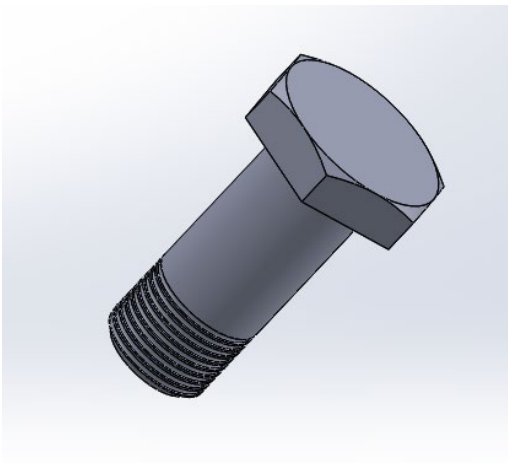

Figure 41: 3-D design of the bolt in SolidWorks

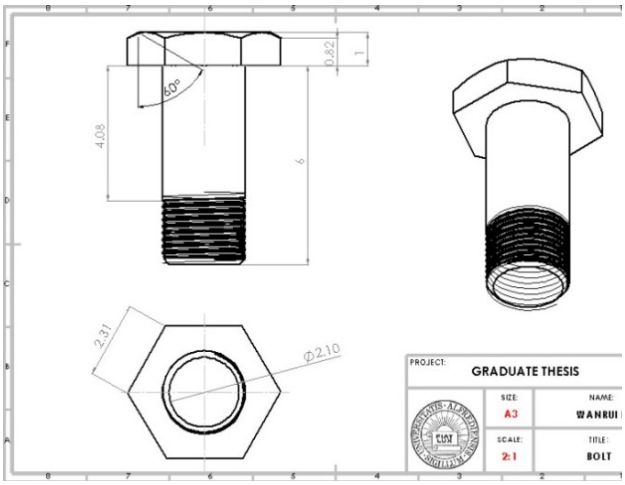

Figure 42: 2-D drawing of the bolt in SolidWorks

Figure 43 is the 3-D design of the nut in SolidWorks. The nut is hexagonal in shape, 1.5 cm in height and 4 cm in width, with a threaded diameter of 2.4 cm for screwing the bolt. Figure 44 is a 2-D drawing of the nut in SolidWorks, it shows three different views of the nut, with all measurements included.

The long pin which connects the different linkages is unchanged from the previous design, as seen in Figures 25 and 26. Because redesigned linkage-one and redesigned linkage-two have only changed in angle θ, their length and width are the same meaning the long pin did not need to be redesigned.

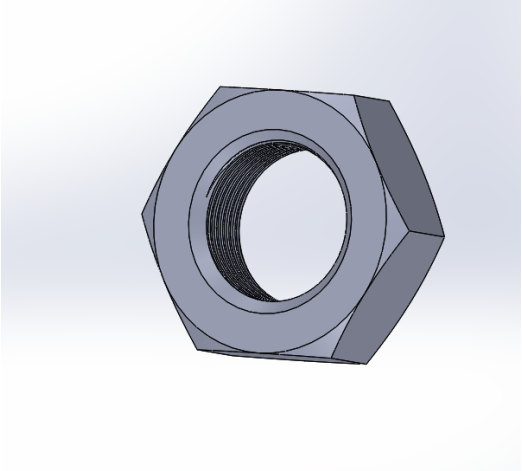

Figure 43: 3-D design of the nut in SolidWorks

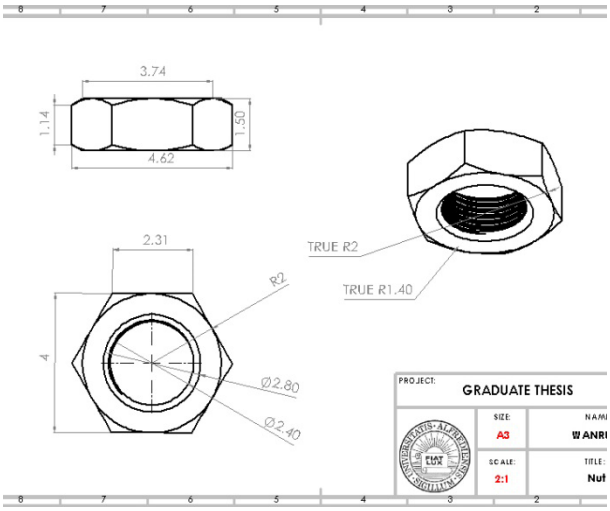

Figure 44: 2-D drawing of the nut in SolidWorks

All redesigned components are shown in Figure 35 through Figure 44 as well as Figure 25. Figure 45 shows the structure and the three axes (x-axis, y-axis and z-axis). Each assembled axis requires the following components; sixteen redesigned linkages-one, sixteen redesigned linkages-two, eight redesigned connectors, sixteen bolts and nuts, and thirty-two long pins, for a total of forty-eight redesigned linkages-one, forty-eight redesigned linkages-two, twelve redesigned connectors, forty-eight bolts and nuts, and one hundred and twenty long pins in the final model. The reason only twelve redesigned connectors, rather than twenty-four, are needed is that any two axes share some redesigned connectors, meaning only twelve redesigned connectors are required to assemble the entire sphere. Figure 46 is a two-dimensional drawing of the sphere structure in SolidWorks, with three different views shown.

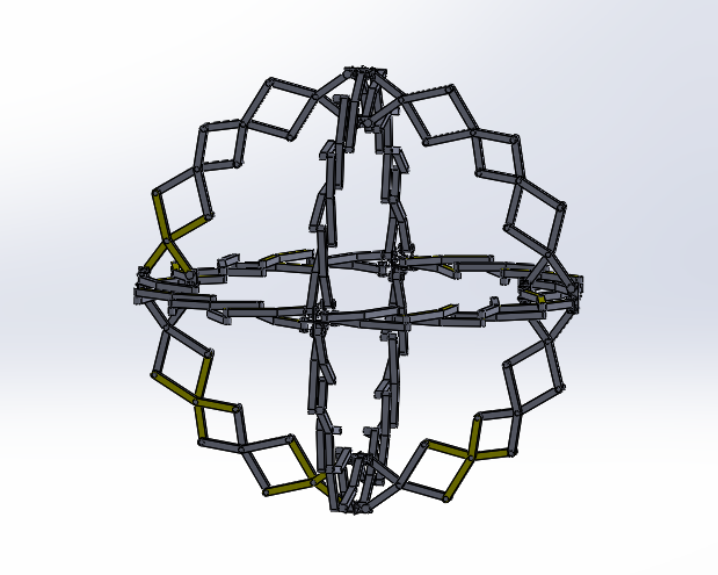

Figure 45: 3-D design of the redesigned assembly model in SolidWorks

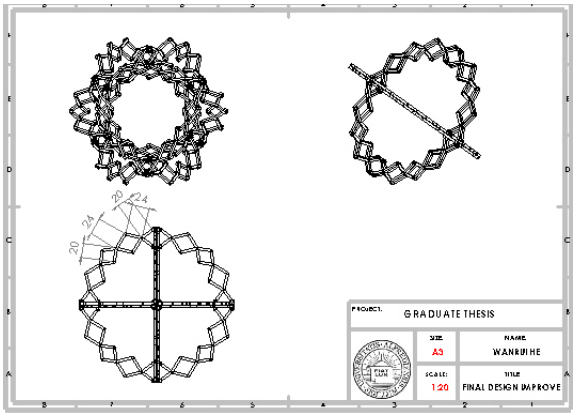

Figure 46: 2-D drawing of the redesigned assembly model in SolidWorks

D. FEA Analysis

1. Brief Introduction of Finite Element Analysis on ANSYS Workbench

Finite Element Method（FEM）is a numerical technique for solving approximate solutions of partial boundary value problems. When solving, the entire problem area is decomposed. Each sub-area becomes a simple part. This simple part is called a finite

element. It uses a variational method to minimize the error function and produce a stable solution.[11] Analogous to the idea of connecting multiple segments of a small straight line approximation, the finite element method contains all possible methods, which link many simple equations in small regions known as finite elements and use them to estimate complex equations over larger regions. It considers the solution domain to be composed of many small interconnected subdomains called finite elements, and assumes a suitable (simpler) approximate solution for each element, and then derives the total satisfying conditions for this domain (such as the equilibrium condition of the structure) to get the solution to the problem. This solution is not an exact solution, but an approximate solution, because the actual problem is replaced by a simpler problem. For most practical problems are difficult to get accurate solutions, finite element not only has high accuracy, but also can adapt to various complicated shapes, thus becoming an effective means of engineering analysis.[11]

2. Structure analysis by FEA method (Ansys Workbench)

2.1 Finite element analysis theory

The basic idea of finite element analysis is to discretize the continuous geometric structure into a finite number of units, and set finite nodes in each unit so that the continuum is regarded as a group of units connected only at the nodes. At the same time, the node value of the field function is selected as the basic unknown quantity, and an approximate interpolation is assumed in each unit to represent the distribution law of the field function in the unit, and then the finite element equations for solving the unknown node quantity are established. The problem of infinite degree of freedom in a continuous domain is

transformed into a finite degree of freedom problem in discrete domain. After the node value is obtained, the field function on the unit and even on the whole assembly can be determined by the set interpolation function. In the finite element discretization process, adjacent elements are continuous at the same node, but not necessarily at any point in the boundary. In the process of transforming the load into node load, only the overall cell balance is considered, and there is no need to ensure that every point satisfies the governing equation in the interior and boundary of the element.[11] The basic steps of finite element analysis are as follows:

1. The solution domain is established and discretized into finite element, which decomposes the continuum problem into individual problems such as nodes and elements.
2. Assuming the function representing the physical behavior of the unit, that is, the approximate continuous function representing the solution of the unit;
3. Establishing the element equation;
4. Constructing the whole stiffness matrix of the unit;
5. Imposing boundary conditions, initial conditions and loads;
6. Solving linear or nonlinear differential equations, the nodal solution results are obtained.

2.2 Purpose of Finite Element Analysis (FEA)

Why choose FEA? The reason is this dissertation is designed in a more complex structure. FEA can completely obtain its accurate internal mechanical information under the action of the complex external forces, i.e., to obtain the three types of mechanics information (displacement, strain and stress) of the deformation body. Based on accurate mechanical analysis, the structure of the design can be evaluated in strength, stiffness, and

other aspects, thus to modify unreasonable design parameters to obtain a more optimal design. Next, the FEA after the program modification should be performed again for final mechanics evaluation and verification to determine the final design plan. Another reason is compared with other analysis methods, the finite element method has the following advantages:

1) Be able to analyze complex structures. Since the discrete element is not limited to a uniform regular cell, the cell shape has certain arbitrariness, and the cell size may be different, and the cell boundary may be curve or camber. Therefore, the analytical structure may have a very complicated shape, which may not only be a complicated planar structure or axisymmetric structure, but also can be a three-dimensional cage structure or a physical structure.
2) Be able to handle complex boundary conditions. In the finite element method, the boundary condition does not need to introduce the characteristic equation of each element, but the relevant characteristic matrix is processed as necessary after the algebraic equation of the entire structure is obtained, so the same field variable function is adopted for the internal and boundary elements. When the boundary conditions are changed, the field variable function does not need to be changed, so the processing and programming of boundary conditions is very easy.[12]
3) Be able to guarantee the specified accuracy. As the order size decreases or the order of the interpolation function increases, the finite element solution converges to the exact solution of the actual problem. Therefore, the exact

solution to actual problems is converged by the finite element when the single size is reduced or the order of the interpolation function is increased.[12] Therefore, the accuracy of the solution can be improved through grid encryption or high-order interpolation function can be used for improving the accuracy of the solution, so that the analytical solution has a certain value of use.

4) Be able to handle different types of materials. The finite element method can be used for analysis of various types of materials such as isotropic materials, orthotropic materials, anisotropic materials, and composite materials, as well as the analysis of composite structures composed of different materials.

3. ANSYS software

ANSYS is the software been chosen to analysis the model, because the ANSYS software is a general finite element software which integrates the structure, fluid, electromagnetic field, sound field and coupling field analysis. Developed by ANSYS, the largest finite element analysis company in the world, it can share and exchange data with most CAD software. ANSYS was founded in 1970, headquartered in Pittsburgh, Pennsylvania, USA, dedicated to the research and development of CAE technology. Now the ANSYS software has been successfully applied in every field of the world. It is a powerful and flexible software package for design analysis and optimization. You can float a variety of computers and operating systems running from PCs to workstations to supercomputers.[8]

To analysis a sports model, there is an analysis system in ANSYS called transient structural, transient dynamic analysis (also called time process analysis) is a method for determining the dynamic response of structures subjected to arbitrary time-varying loads. The transient dynamic analysis can be used to determine the time-varying displacement, strain, stress and force of the structure under the random combination of steady load, transient load and simple harmonic load.[13] This system is the best way to analysis the project model.

The correlation between load and time makes inertial force and damping become more vital. If the inertial force and damping are not important, the transient analysis can be replaced by static analysis. The basic equations of motion of transient dynamics are [13]:

$$[M]\{\ddot{u}\} + [C]\{\dot{u}\} + [K]\{u\} = \{F(t)\} \tag{28}$$

$[M]$ = Mass matrix

$[C]$ = Damping matrix

$[K]$ = Stiffness matrix

$\{\ddot{u}\}$ = Node acceleration vector

$\{\dot{u}\}$ = Node speed vector

$\{u\}$ = Node displacement vector

Transient structure analysis is given by the above formula and is tackled in this paper in five separate sections: Engineering Data, Geometry, Model, Setup and Solution. After setting up all the variables, the program was run to obtain results from the model.

3.1 Engineering Data

Engineering Data is a resource for material properties used in an analysis system, it is designed to create, save, and retrieve material models, as well as to create libraries of data that can be saved and used in subsequent projects and by other users. Engineering Data can be shown as a component system or as a cell in any mechanical analysis system. As a standalone component system, the workspace accesses all material models and properties by default. When viewed as a cell in a mechanical analysis system, the workspace shows that material models and properties pertinent to that system's physics.[15]

The material that been chosen for this project model is Structural Steel, the reason why to chosen steel, because it is ANSYS system default material. The density of Structural Steel is 7850 kg m^-3, it is a high-strength material. Table I and II are properties of Structural Steel. Table I shows the isotropic elasticity of Structural Steel, the value of Young's modulus, Poisson's ratio, Bulk modulus and shear modulus are system default when the material had been chosen. Table II shows the strain-life parameters of Structural Steel, all value also are system default when the material had been chosen. Other properties' values of Structural Steel are tensile yield strength 2.5E+8 Pa, compressive yield strength 2.5E+0.8 Pa, tensile ultimate strength 4.6E+8 Pa, and compressive ultimate strength 0 Pa. All values were got from engineering data.

Table I: Properties of Isotropic Elasticity for Structural Steel

Isotropic Elasticity	Value	Unit
Young's Modulus	2E+11	Pa

Poisson's Ratio	0.3	
Bulk Modulus	1.6667E+11	Pa
Shear Modulus	7.6923E+10	Pa

Table II: Properties of Strain-Life Parameter for Structural Steel

Strain-Life Parameters	Value	Unit
Strength Coefficient	9.2E+8	Pa
Strength Exponent	-0.106	
Ductility Coefficient	0.213	
Ductility Exponent	-0.47	
Cyclic strength Coefficient	1E+9	Pa
Cyclic Strain Hardening Exponent	0.2	

3.2 Geometry setup

The second step of the transient setup was to define the modelling geometry for SolidWorks. Next, the model was imported from SolidWorks and all connections set up, as shown in Figure 47. This imported model retains the size of the model in SolidWorks, but the bolts and nuts were hidden for the geometric setup. Figure 47 features three different color arrows, with the red arrow representing the X-axis, the green arrow the Y-axis, and the blue arrow the Z-axis. To set up the model's connections, revolute must be used to arrange the joints. Firstly, the model was split into twelve sections, each with fourteen revolute joints. Each revolute joint must arrange one face as a reference scope and another

as a mobile scope. After setting up all the revolute joints for each section, the model has the directions shown in Figure 47. These directions were established according to the revolute joints, but the directions of the X, Y, and Z-axes are not affected by the model analysis, and hence, their arrows point in different directions.

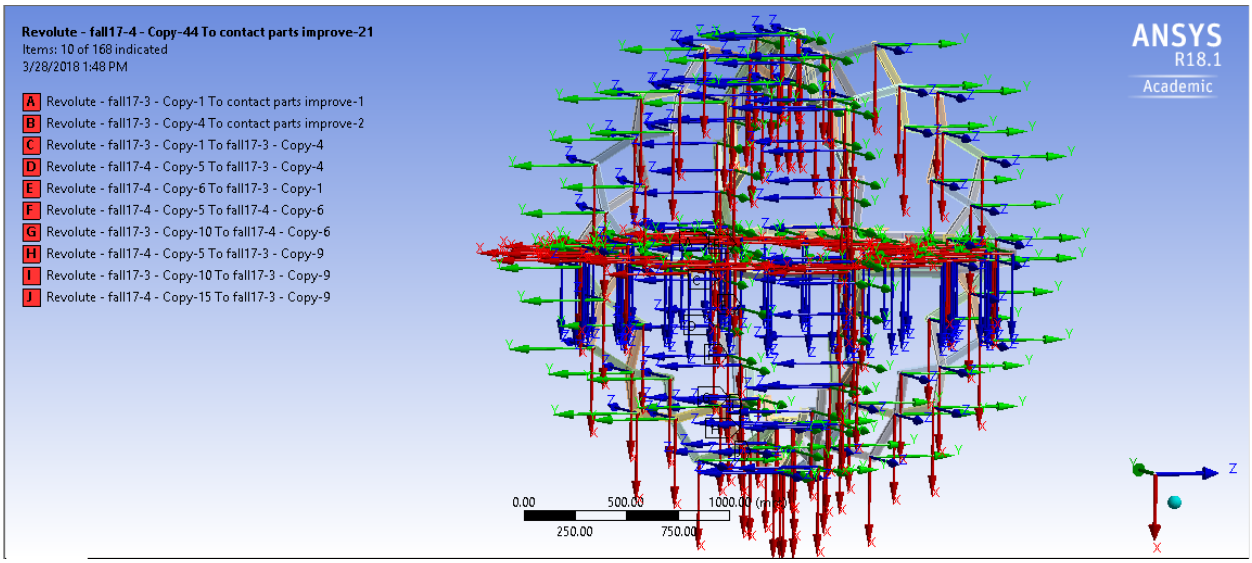

Figure 47: Set up of project model connections

3.3 Meshing Procedure

ANSYS meshing is an important step for set up the program, because the solid model cannot be directly used for finite element calculation, so it needs to be meshed to generate a finite element model. The finite element model is a mathematical representation of the actual structure and material. In ANSYS, a unit to divide the solid model to produce a finite element model, this process is called meshing of the solid model. In essence, meshing the solid model is to divide the solid model into multiple sub-areas using one unit.[17] These sub-regions (units) are attributes, that is, the previously set cell attributes. It is also possible to directly generate finite element models using elements and nodes.

In ANSYS meshing, there are various mesh types, with different types of unit applied to different types of analysis, different materials and different geometries. Therefore, the correct choice of mesh type is very important. The most common types are the 2-D planar element and 3-D solid element.

The 2-D planar element has triangular and quadrilateral elements, with 3 nodes, 4 nodes, 6 nodes, and 8 nodes. They are generally used for plane analysis or axisymmetric section analysis. The plane problem's geometric model must be built in the XY plane. Figure 48 shows four element types and outlines their displacement functions.

Type of Element	Displacement function
Linear Tria 3  CST (Constant Strain Triangle)	$u = a_0+a_1x+a_2y$ (3 nodes – 3 terms in displacement function) Strain = $\varepsilon_x = \frac{\partial u}{\partial x} = a_1 = \text{const.}$ $\varepsilon_y = \frac{\partial u}{\partial y} = a_2 = \text{const.}$
Linear Quad 4 	$u = a_0+a_1x+a_2y+a_3xy$ (one additional term in comparison to tria 3, makes it more accurate)
Parabolic Tria 6  LST (Linear Strain Triangle)	$u = a_0+a_1x+a_2y+a_3x^2+a_4y^2+a_5xy$ (6 nodes – 6 terms in displacement function)
Parabolic Quad 8 	$u = a_0+a_1x+a_2y+a_3xy+a_4x^2+a_5y^2+a_6x^2y+a_7xy^2$ (two additional terms in comparison to tria 6, makes it more accurate)

Figure 48: Different element types and their corresponding displacement functions for 2-D planar meshing.[18]

The 3-D solid elements' types are tetrahedron and hexahedron, and the number of nodes varies from 4 to 20, which is suitable for different type of analysis and accuracy.

Tetrahedron meshing builds 4 and 10 nodes tetras, it can be created through the edit element panel, tetra mesh panel, and shrink wrap panel, and it is showing in Figure 49. Hexahedron meshing builds 8 and 20 nodes hexa elements, shows in Figure 49, and it can be built in any of the following panels[19]:

- Drag: drags a group of two-dimensional elements along a vector to create solids.
- Edit element: builds elements by hand
- Line drag: drags a group of two-dimensional elements along a line.
- Linear solid: creates solid elements between two-dimensional elements
- Solid map: builds solid elements between nodes, lines and surfaces
- Solid mesh: builds solid elements between a variable number of lines
- Element offset: creates solid elements by offsetting a group of two-dimensional elements normal to the surface formed by the group of two-dimensional elements
- Spin: spins a group of two-dimensional elements about a vector to create solid elements
- Split: propagates split hexas

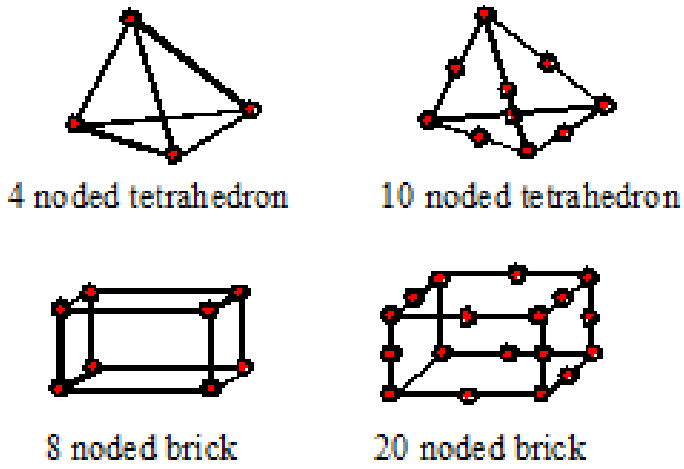

Figure 49: Different nodes in type of tetrahedron and hexahedron elements in 3-D solid meshing

For this project model, 3-D solid meshing should be chosen, because this mesh is between tetrahedron and hexahedron elements, each of which has different advantages and disadvantages. For tetrahedral mesh, the advantages are good adaptability for complex geometries, appropriate for free meshing, and speed of mesh production. Meanwhile, its disadvantages are that, for the same size, the result is less accurate than it is for hexahedron mesh, which requires higher-order units to be used, leading to greater calculations. For hexahedral mesh, the advantages are small calculation scale and appropriateness for dynamic analysis; while its disadvantages are the increased time taken for geometry simplification, cutting, and long grid generation. For this model, hexahedral meshing was the optimal choice, with an element size of 10 mm, and a total of 420453 nodes and 72041 elements. Figure 50 shows the model after the meshing was created. Meanwhile, figure 51 shows the hexahedral elements meshed together in the model, with linkages meshed equally, while elements close to the joints are more irregular. Once the meshes were created, the transient structural simulations could be run.

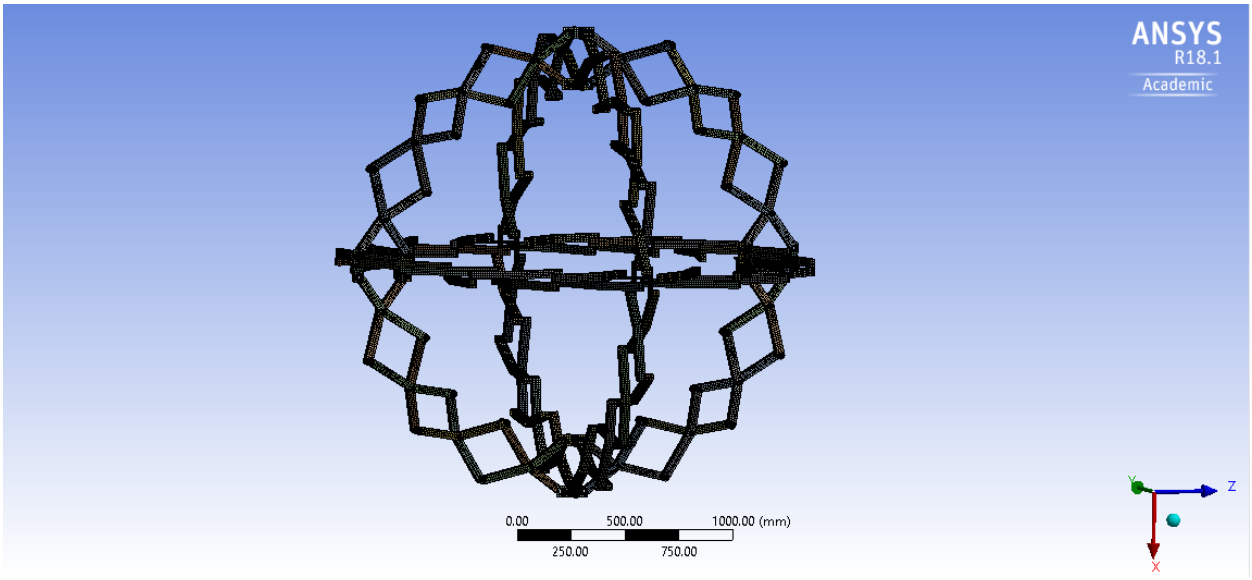

Figure 50: Mesh created in ANSYS

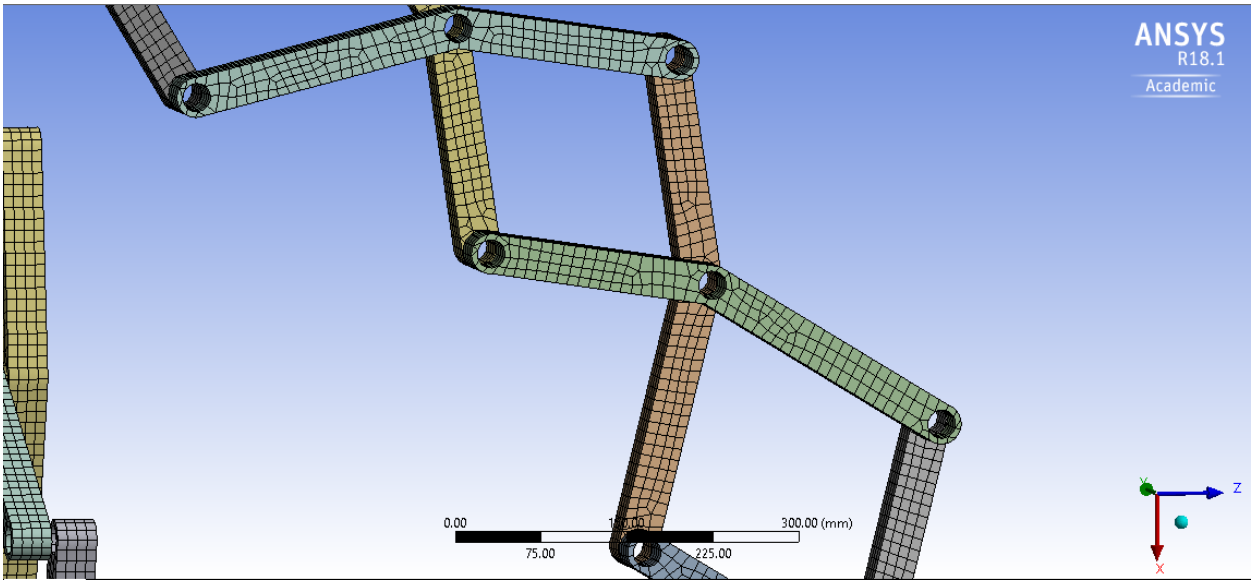

Figure 51: Magnified view of the mesh created zoom in ANSYS

3.4 Transient setup

The last step set up the transient, with the most importing settings being analysis settings. The number of steps was 1, the step end time was 1 second, and with auto timed stepping enabled, substeps could be defined. Certain other important values also needed to

be set up, with the initial substeps at 50, the minimum substeps at 20 and the maximum substeps at 10000, with time integration turned on. This model is symmetric, meaning two symmetrical displacements needed to be added to the model. Table III shows the model's Y-axis displacement, with a value of -300 because it extended into the negative quadrant, while the values of the X and Z- axes were 0, meaning there was no displacement.

Table III: Displacement values for the model

Steps	Time [s]	X [mm]	Y [mm]	Z [mm]
1	0	0	0	0
	1	0	-300	0

Table IV shows another displacement on the Y-axis, with a value of 300 because it occurred in the positive quadrant, while the values of the X and Z- axes were 0, meaning there no was displacement. After setting up all the variables, the program was ready to run.

Table IV: Displacement 2 values for the model

Steps	Time [s]	X [mm]	Y [mm]	Z [mm]
1	0	0	0	0
	1	0	300	0

IV. RESULTS AND DISCUSSION

Before to use ANSYS to do finite element analysis (FEA), the 3-D model printed out was analyzed. It was found that the design in this paper could change the size of the structure. To exert force outwards on any node could get the model expanded. Similarly, to exert a force in the opposite direction on any node could compress the model. The force exerted was decided by the size and materials of the model. A major advantage of the design in this paper was that the structure could change its own size to get adapted to spaces and environments of different sizes. Two stable configurations constituted main characteristics of this structure. It could be fully folded or fully expanded to get tasks accomplished. Under the folded status, the structure had a small volume, which was convenient for storage and to work in a small space. A major defect of the design in this paper was that, under the external driving force, the structure could gradually get expanded fully and stay at a stable status. However, during the process of expansion, the design structure was an unstable system, which required ANSYS to analyze the movement trace, time, speed, deformation and strain changes of the structure in the process. Therefore, this paper conducted ANSYS to do FEA of this design for the purpose of gaining a better understanding of advantages and disadvantages of the design in this paper.

When running a program, it is possible to obtain results for deformation, strain, stress and energy. Then, the most relevant results can be identified and analyzed according to the model's purpose. To analysis this project model, several aspects are needed, which are total deformation, equivalent stress, and force reaction.

Total deformation is calculated for the component or assembly world coordinate system. Physical deformation can be calculated on or inside of a component or an assembly. To calculate total deformation, scoping was required for both geometric and underlying meshing entities, while numerical data was obtained for measuring deformation in the global X, Y, and Z directions. Figure 52 shows three component deformations U_x, U_y, and U_z, with the deformed U-shape available from the individual results, and the formula showing the calculation of total deformation. The blue arrows represent component deformational (directional deformation), while the red arrows represent the deformed shape (total deformation vector).

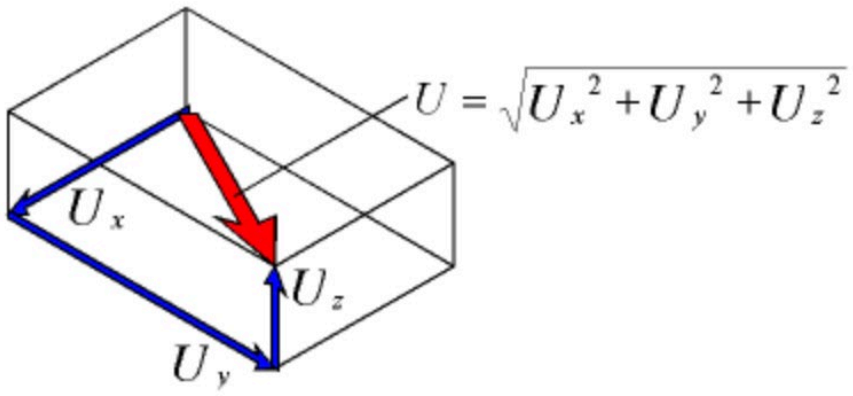

Figure 52: Deformation theory diagram

Equivalent stress (otherwise known as von Mises stress) allows any arbitrary 3D stress state to be represented as a single positive stress value. Equivalent stress is also part of maximum equivalent stress failure theory, which is used to predict yield in ductile

materials. During design, equivalent stress served as a good value for analyzing this project model. Equivalent stress is related to principal stress by equation [20]:

$$\sigma_e = \left[\frac{(\sigma_1 - \sigma_2)^2 + (\sigma_2 - \sigma_3)^2 + (\sigma_3 - \sigma_1)^2}{2}\right]^{1/2} \quad (29)$$

The equivalent strain ε_e is computed as [20]:

$$\varepsilon_e = \frac{1}{1+v'}\left(\frac{1}{2}[(\varepsilon_1 - \varepsilon_2)^2 + (\varepsilon_2 - \varepsilon_3)^2 + (\varepsilon_3 - \varepsilon_1)^2]\right)^{1/2} \quad (30)$$

Where:

v' = effective Poisson's ratio, is defined as a material Poisson's ratio for elastic and thermal strains computed using the body as a reference temperature. According to the formulas shown above, when equivalent stress increases, the material grows weaker, signaling the model to be unsafe.

Force reaction is the vector sum of the selected portion's fulcrum forces. It shows the force changes on the X, Y, and Z-axes over time. By analyzing the force reaction, the degree of force loaded on the model can be determined.

Figure 53 shows the impact of total deformation on the model. The color bar on the left hand side shows the different total deformation values, with navy blue corresponding to the minimum total deformation, 278.7 mm, while the red corresponds to the maximum total deformation, 429.78 mm. Navy blue is mostly prominently shown on the outskirts of the model, meaning this are experienced minimal total deformation, while the inner part is mostly red, meaning it experienced maximum total deformation. After the time fully

elapsed, the total deformation values from minimum to maximum are displayed on the model.

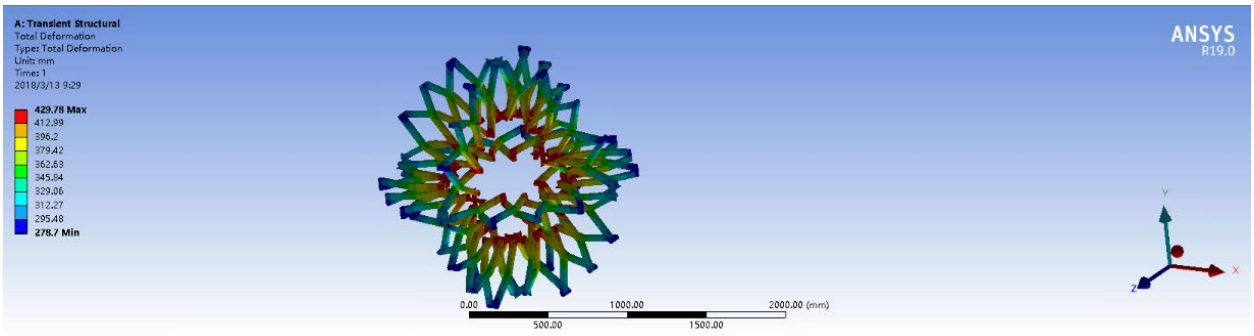

Figure 53: Total deformation of the designed model in ANSYS

Figure 54 shows the total deformation plot with transient time and the designed model's deformation. Transient time (s) is on the x-axis, with total time set to one second. Meanwhile, the y-axis shows the deformation (mm), with the minimum deformation at 2.1164 mm and the maximum deformation at 429.78 mm. The green line on the graph is the Y-axis, the blue line the Z-axis, and the red line the X-axis. As total deformation increases with time, it increases across all axes (X, Y, and Z). When time equals one second, the total deformation on the Y-axis is at its maximum.

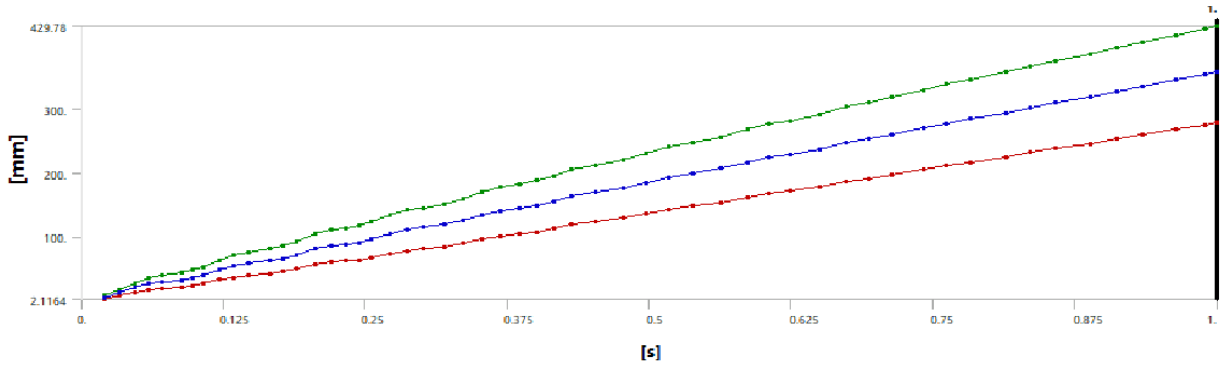

Figure 54: Total deformation plot with time (s) and deformation (mm) of the designed model in ANSYS

Figure 55 shows the result of equivalent stress for the model. The color bar on the left hand side shows the different equivalent stress values, with navy blue corresponding to the minimum equivalent stress, 4.0101e-5 MPa, while red corresponds to the maximum equivalent stress, 11.329 MPa. Navy blue is most prominent on the model's outskirts, meaning this area had minimum equivalent stress, while the inner part is mostly red, meaning it had maximum equivalent stress. After the time elapsed, the equivalent stress values obtained are shown for the model, from minimum to maximum.

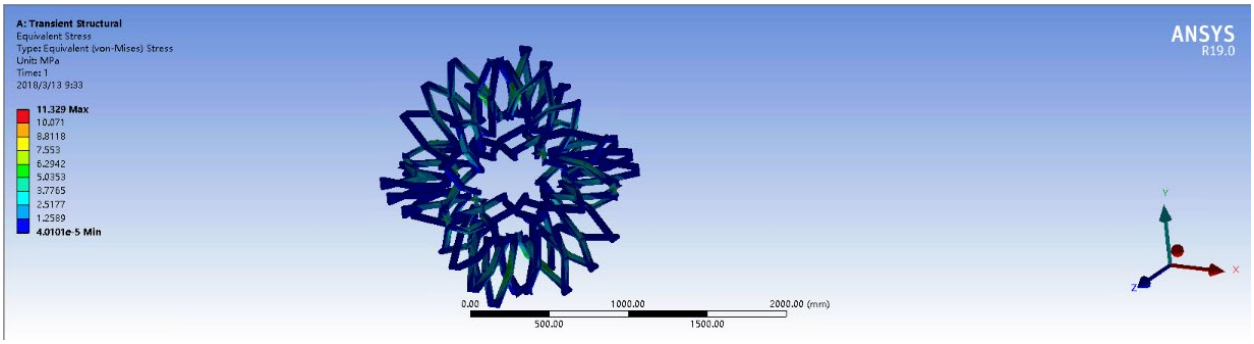

Figure 55: Equivalent stress of the designed model in ANSYS

Figure 56 is an equivalent stress plot with transient time and stress of the designed model. Transient time (s) is shown on the X-axis, with total time set to one second. Meanwhile, the y-axis shows equivalent stress (MPa), with a minimum equivalent stress of 3.5805e-05 MPa and a maximum equivalent stress of 107.85 MPa. The green line is the Y-axis, the blue line the Z-axis, and the red line the X-axis. The red line did not record any changes over time. Instead, it stayed at the minimum value, meaning the equivalent stress on the X-axis did not change. The blue line recorded a weak decrease over time increases,

with its value close to minimum but not yet there, meaning the equivalent stress caused a small change in the Z-axis. The green line irregular decreased over time, meaning the equivalent stress caused its greatest change in the Y-axis. During step time, some equivalent stress points achieved minimum and maximum values.

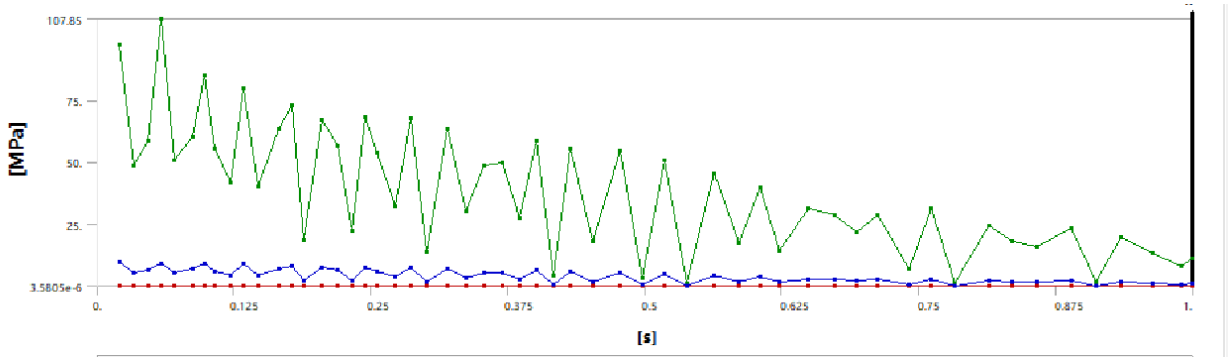

Figure 56: Equivalent stress plot with time (s) and stress (MPa) of the designed model in ANSYS

Figure 57 shows force reaction for the model's first displacement. The blue arrow shown above represents the displacement that loaded the model.

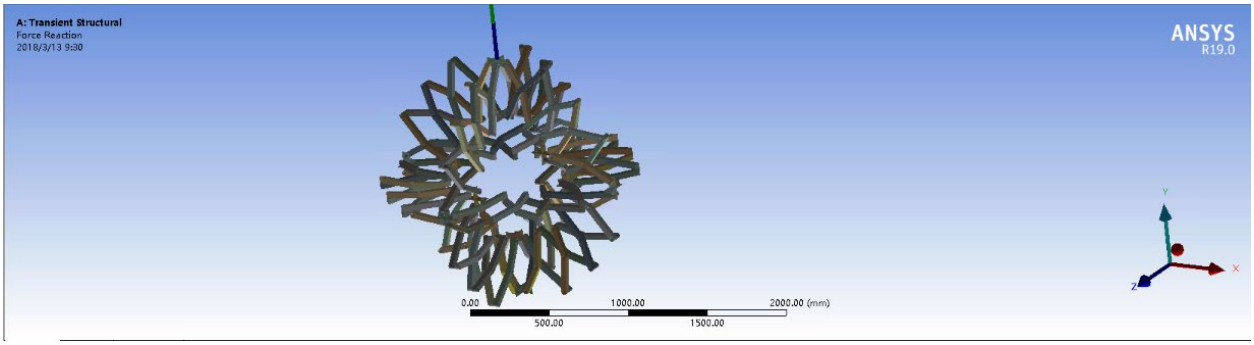

Figure 57: Force reaction of the designed model in ANSYS

Figure 58 shows the first displacement of the force reaction plot with transient time and force of the designed model. Transient time (s) is shown on the X-axis, with total time set to one second. Meanwhile, force (N) is on the Y-axis, with the model's minimum force recorded at -10680 N and maximum force at 15209 N. The green line is the Y-axis, the

blue line the Z-axis, and the red line the X-axis. The blue line did not record any changes over time, staying at zero, meaning no force reactions were felt on the Z-axis. The red line shows the force reaction on the X-axis changed in the positive quadrant. Moreover, time equaled 0.0625 s, the force reaction was at its maximum, meaning the force reaction on the X-axis only changed positively. The green line was changed on both the positive and negative sides of the graph, with irregular changes occurring over time, meaning the force reaction on the Y-axis fluctuated in the positive and negative directions.

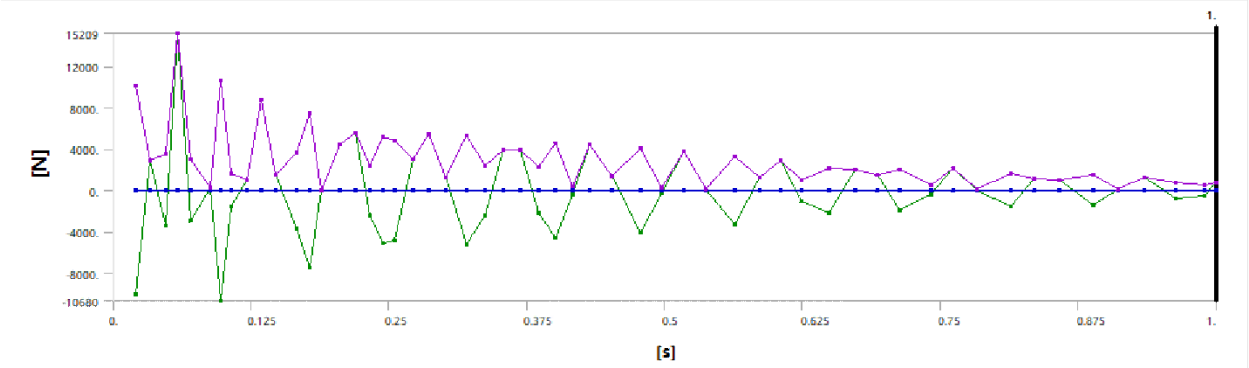

Figure 58: Force reaction plot with time (s) and force (N) of the designed model in ANSYS

Figure 59 shows the force reaction of the model's second displacement. The blue arrow shown at the bottom was caused by the displacement that loaded the model.

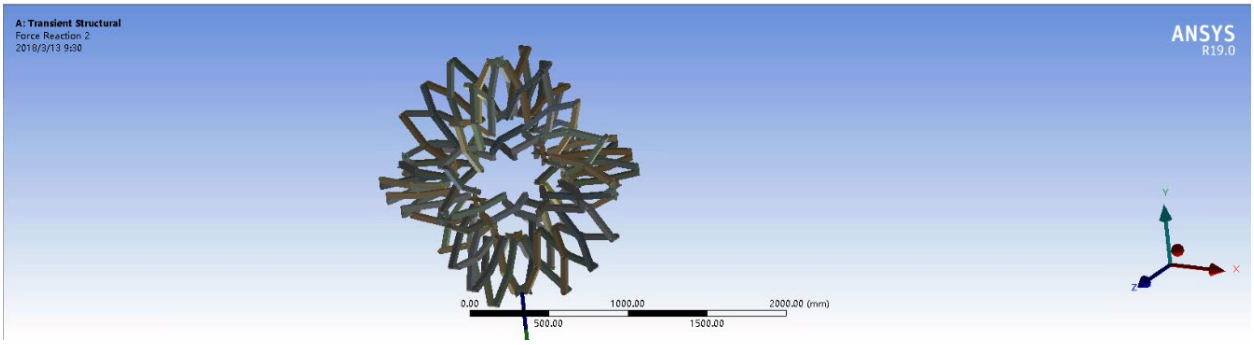

Figure 59: Force reaction 2 of the designed model in ANSYS

Figure 60 shows a second displacement of force reaction plot with transient time and force of the designed model. Transient time (s) is shown on the X-axis, with total time set to one second. Meanwhile, force (N) is on the Y-axis, with a minimum force of -15209 N and a maximum force of 15209 N. The green line is the Y-axis, the blue line the Z-axis, and the red line the X-axis. The blue line did not record any changes over time, staying at zero, meaning there was no force reaction felt on the Z-axis, like it was for the first force reaction. The red line shows the force reaction on the X-axis was changed in the positive quadrant. When time equaled 0.0625 s, the force reaction was at the maximum, meaning the force reaction on the X-axis was only changed in the positive direction. The green line changed on both the positive and negative sides of the graph, with irregular changes over time, meaning the force reaction on the Y-axis changed in the positive and negative directions. However, when time equaled 0.0625 s, the force reaction was at the minimum, while the force reactions on the X-axis and Y-axis were exactly the opposite, meaning the forces exerted on the X-axis and Y-axis were equal but acted in opposite directions.

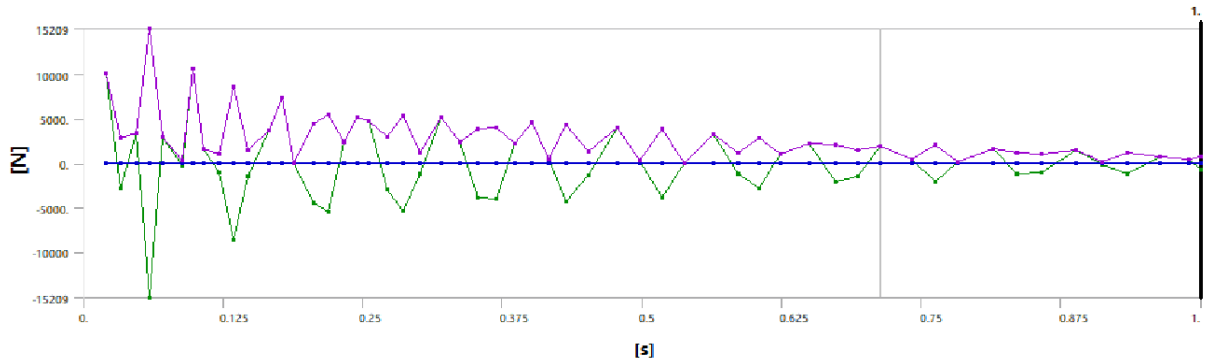

Figure 60: Force reaction 2 plot with time (s) and force (N) of designed model in ANSYS

V. SUMMARY AND CONCLUSIONS

This study aimed to design a rescue robot structure, which could allow the robot to work under different post-disaster environments. The appearance design of the rescue robot featured a spherical structure, which could adjust the body size of the rescue robot according to different sizes of the environment space. In this way, the rescue robot would be able to work in different sizes of space. In this design, the spherical structure could be spread into a structure with a diameter of 114.18 cm. The compression size was decided by the post-disaster environmental space. Test of the 3D printed model showed that the force could be exerted on any linkage or junction of the spherical structure to spread or compress the structure. Besides, the size of the included angle between arms and the number of linkages could be changed to change the size of the sphere. Therefore, this design was not restricted to one size.

After a disaster happens, the disaster-stricken environment is usually complex. Many irregular obstacles or uneven roads might influence the work of the rescue robot. This design could change the size of robot when encountering an obstacle. If the volume of an obstacle was larger than the rescue robot after being spread, the rescue robot could compress its body size to seek other narrower space to pass through. On the contrary, when the obstacle volume was smaller than the rescue robot after being compressed, the rescue robot could span over the obstacle. These were two major concerns of the rescue robot design in this paper.

In order to test feasibility of the design in the real life, ANSYS was adopted for a finite element analysis of the transient structure from the perspective of total deformation and equivalent stress. The maximum total deformation of the spherical structure was

429.78 mm. It was mainly distributed within the structure. The minimum total deformation was 2.1164 mm. It was mainly distributed in the periphery part of the structure. The maximum equivalent stress was 107.85 MPa, which was mainly distributed within the structure, while the minimum was 3.5805e-05 MPa, which was mainly distributed in the periphery part of the structure. Numerical and image analysis suggested that the structure underwent none crack or rupture. This meant the structure could bear certain degree of external force during the spreading or compression process.

VI. FUTURE WORK

This paper designed an external structure for the rescue robot. Considering limitations of this research, the author will deepen research in the following aspects. First, the redesigned assembly model will be made by 3D printing to test the direct connection problems of linkages. Second, ANSYS will be used to test numerical changes of the model deformation and stress with different materials adopted. Based on the test results, the most suitable material will be chosen to build this design, and the design will be verified under the practical conditions. In this paper, the rescue robot external structure design failed to link hardware with software. In the future, the author will consider how to use coding to enable automatic spreading and compression of the spherical structure during the movement process. Besides, the author will also investigate the situation when the rescue robot suffers the secondary aftershock.

REFERENCES

1. "HOBERMAN Transformable design" (2010) Hoberman Associates, Inc. Accessed on: November 2017. Available at <http://www.hoberman.com/history.html>

2. Li B. The research of snake robot and its app location in disaster rescue operations. Robot Technique and Application, 2003, (3): 22-26

3. Jennifer Casper, Robin Roberson Murphy. Human-robot interactions during the robot assisted urban search and rescue response at the World Trade Center. IEEE Transactions on systems, man, and cybernates Part B: Cybernetics, 2003, 33 (3): 367-385

4. Charles Hoberman, Connections to make foldable structures US 20020083675 A1, 4 July 2002, US 09/766,242

5. Sarah Bolton, Dominic Doty and Peter Rivera, "Compact Deployable Antenna for CubeSat Units," A Senior Project Sponsored by NASA's Jet Propulsion Laboratory, Ch. 2 pp. 12. Mechanical Engineering Department California Polytechnic State University, San Luis Obispo (2014-2015).

6. Sunil K. Agrawal, Saravana Kumar, Mark Yim and John W. Suh, "Polyhedral Single Degree-of-freedom Expanding Structures," Department of Mechanical Engineering, University of Delaware; Members of Research Staff, Xerox Palo Alto Research Center.

7. S. Pelligrino and Z. You, "Foldable Bar Structures," International Journal of Solid Structures, vol. 34, no. 15, pp. 1825-1847, 1997.

8. Maxwell H. Wolfe, "Analysis of Deployable Strut Roof Structures," Ch.5 pp. 23-25, B.S. Civil Engineering Northeastern University, 2012

9. Jiten Patel and G.K. Ananthasuresh, “A kinematic theory of radially foldable planar linkages,” Mechanical Engineering, Indian Institute of Technology-Madras, Chennai 600036, India; Mechanical Engineering, Indian Institute of Science, Bangalore 560012, India, 2007

10. Hunt, K.H., 1978. “Kinematic Geometry of Mechanisms”. Oxford University Press.

11. School of Mechanical and Automotive Engineering Zhejiang University of Science and Technology. “The curvature of conjugated gear finite element analysis of bending stress”. 2012

12. Zhongwen Huang, “Heat exchanger coupled thermal stress analysis”. 2015

13. Rao Cong, Bo Zhitao, and Lu Lin, “Two-layer Deployable Objects Modeling based on Scissor Structures”. School of Computer Science and Technology, Shandong University, Ji’nan 250101

14. Yang Xiaolan, Liu Jifeng and Chen xuan, “Analysis of ANSYS Finite Element Mesh Dividing”. Nanjing Institute of Technology, Nanjing 210013, China

15. Steve Hale, CAE Associates, Inc. “Managing Material Property Data with the Workbench Engineering Data Manager” 2012 CAE Associates.

16. Zhao J S, Chu F, Feng Z J. The mechanism theory and application of deployable structures based on SLE[J]. Mechanism and Machine Theory, 2009, 44(2): 324-335

17. Li Qingling, “Study of Mesh Dividing Methods in ANSYS”, School of Mechanical, Shanghai Dianji University, Shanghai, 200245

18. “2D Meshing”, Altair University, 2014

19. “3D Meshing”, Altair University, 2014

20. https://www.sharcnet.ca/Software/Ansys/17.0/en-us/help/wb_sim/ds_Equiv_Stress.html

21. Mark Micire, “Analysis of the robotic-assisted search and rescue response to the world trade center disaster” College of Engineering University of South Florida, July 17, 2002

APPENDIX

Table 5

Model (A4) > Coordinate Systems > Coordinate System

Object Name	*Global Coordinate System*
State	Fully Defined
Definition	
Type	Cartesian
Coordinate System ID	0.
Origin	
Origin X	0. mm
Origin Y	0. mm
Origin Z	0. mm
Directional Vectors	
X Axis Data	[1. 0. 0.]
Y Axis Data	[0. 1. 0.]
Z Axis Data	[0. 0. 1.]

Table 6

Model (A4) > Connections

Object Name	*Connections*
State	Fully Defined
Auto Detection	
Generate Automatic Connection On Refresh	Yes
Transparency	
Enabled	Yes

Table 7

Model (A4) > Connections > Joints

Object Name	*Joints*	*Joints 2*	*Joints 3*	*Joints 4*	*Joints 5*	*Joints 6*	*Joints 7*	*Joints 8*	*Joints 9*	*Joints 10*	*Joints 11*
State	Fully Defined										
Definition											
Connection Type	Joint										

Scope	
Scoping Method	Geometry Selection
Geometry	All Bodies
Auto Detection	
Tolerance Type	Slider
Tolerance Slider	0.
Tolerance Value	9.4383 mm
Use Range	No
Group By	Bodies
Search Across	Parts
Fixed Joints	No
Revolute Joints	No
Statistics	
Connections	14
Active Connections	14

Table 8

Model (A4) > Connections > Joints 12

Object Name	*Joints 12*
State	Fully Defined
Definition	
Connection Type	Joint
Scope	
Scoping Method	Geometry Selection
Geometry	All Bodies
Auto Detection	
Tolerance Type	Slider
Tolerance Slider	0.

Tolerance Value	9.4383 mm
Use Range	No
Group By	Bodies
Search Across	Parts
Fixed Joints	No
Revolute Joints	No
Statistics	
Connections	14
Active Connections	14

Mesh

Table 9

Model (A4) > Mesh

Object Name	*Mesh*
State	Solved
Display	
Display Style	Body Color
Defaults	
Physics Preference	Mechanical
Solver Preference	Mechanical APDL
Relevance	0
Element Order	Program Controlled
Sizing	
Size Function	Adaptive
Relevance Center	Coarse
Element Size	Default
Mesh Defeaturing	Yes
Defeature Size	Default
Transition	Fast
Initial Size Seed	Assembly
Span Angle Center	Coarse
Bounding Box Diagonal	3775.30 mm
Average Surface Area	5727.30 mm²

Minimum Edge Length	5.0 mm
Quality	
Check Mesh Quality	Yes, Errors
Error Limits	Standard Mechanical
Target Quality	Default (0.050000)
Smoothing	Medium
Mesh Metric	None
Inflation	
Use Automatic Inflation	None
Inflation Option	Smooth Transition
Transition Ratio	0.272
Maximum Layers	5
Growth Rate	1.2
Inflation Algorithm	Pre
View Advanced Options	No
Advanced	
Number of CPUs for Parallel Part Meshing	Program Controlled
Straight Sided Elements	No
Number of Retries	Default (4)
Rigid Body Behavior	Dimensionally Reduced
Triangle Surface Mesher	Program Controlled
Use Asymmetric Mapped Mesh (Beta)	No
Topology Checking	No
Pinch Tolerance	Please Define
Generate Pinch on Refresh	No
Statistics	
Nodes	420453
Elements	72041

Table 10

Model (A4) > Mesh > Mesh Controls

Object Name	*Sweep Method*	*Hex Dominant Method*	*Body Sizing*
State	Fully Defined		
Scope			

Scoping Method	Named Selection		Geometry Selection
Named Selection	Support	Contact	
Geometry			108 Bodies
Definition			
Suppressed	No		
Method	Sweep	Hex Dominant	
Element Order	Use Global Setting		
Src/Trg Selection	Automatic		
Source	Program Controlled		
Target	Program Controlled		
Free Face Mesh Type	Quad/Tri		
Type	Number of Divisions		Element Size
Sweep Num Divs	Default		
Element Option	Solid		
Control Messages		Yes, Click To Display...	
Element Size			10.0 mm
Advanced			
Sweep Bias Type	No Bias		
Defeature Size			Default
Behavior			Soft

Named Selection

Table 11

Model (A4) > Named Selections > Named Selections

Object Name	*Contact*	*Support*
State	Fully Defined	
Scope		
Scoping Method	Geometry Selection	
Geometry	12 Bodies	96 Bodies
Definition		
Send to Solver	Yes	
Protected	Program Controlled	
Visible	Yes	

Program Controlled Inflation	Exclude	
Statistics		
Type	Manual	
Total Selection	12 Bodies	96 Bodies
Suppressed	0	
Used by Mesh Worksheet	No	

Table 12

Model (A4) > Analysis

Object Name	*Transient (A5)*
State	Solved
Definition	
Physics Type	Structural
Analysis Type	Transient
Solver Target	Mechanical APDL
Options	
Environment Temperature	22. °C
Generate Input Only	No

Table 13

Model (A4) > Transient (A5) > Loads

Object Name	*Displacement*	*Displacement 2*
State	Fully Defined	
Scope		
Scoping Method	Geometry Selection	
Geometry	1 Face	
Definition		
ID (Beta)	2889	2890
Type	Displacement	
Base Excitation	No	
Define By	Components	
Coordinate System	Global Coordinate System	
X Component	0. mm (step applied)	
Y Component	Tabular Data	

Z Component	0. mm (step applied)
Suppressed	No
Tabular Data	
Independent Variable	Time

Figure 61

Model (A4) > Transient (A5) > Displacement

Table 14

Model (A4) > Transient (A5) > Displacement

Steps	Time [s]	X [mm]	Y [mm]	Z [mm]
1	0.	= 0.	0.	= 0.
	1.	0.	-300.	0.

Figure 62

Model (A4) > Transient (A5) > Displacement 2

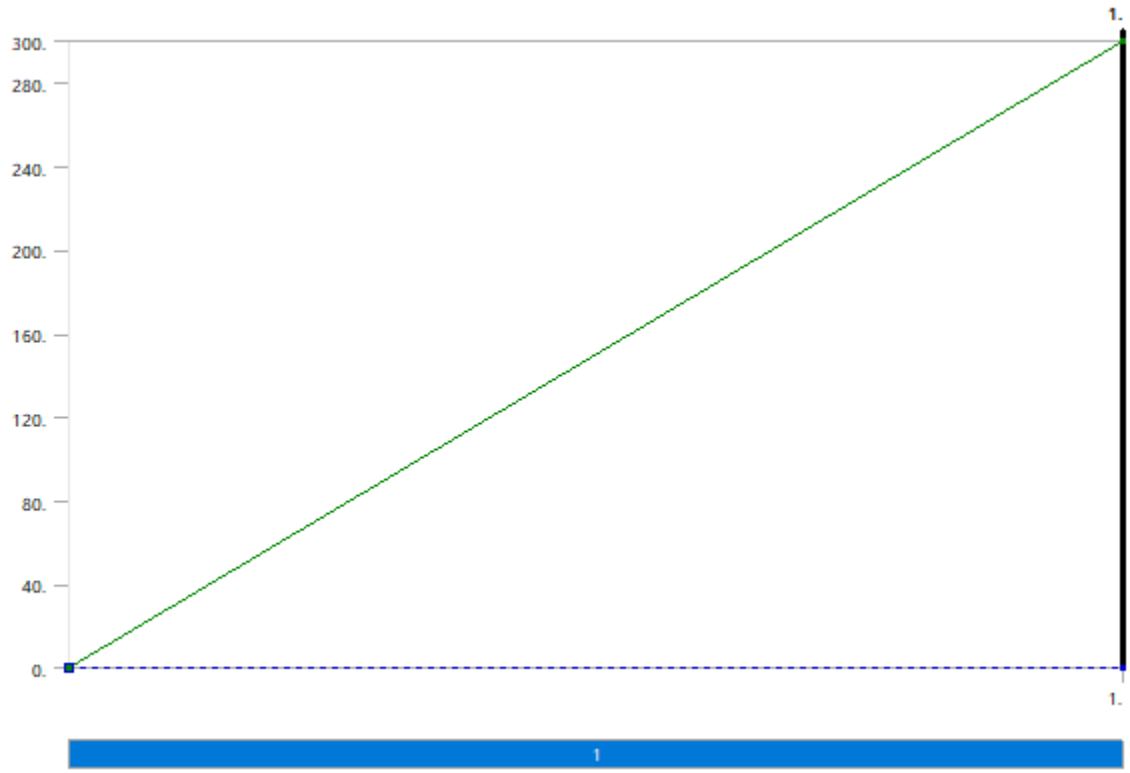

Table 15

Model (A4) > Transient (A5) > Displacement 2

Steps	Time [s]	X [mm]	Y [mm]	Z [mm]
1	0.	= 0.	0.	= 0.
	1.	0.	300.	0.

Solution (A6)

Table 16

Model (A4) > Transient (A5) > Solution

Object Name	*Solution (A6)*
State	Solved
Solution	
Number Of Cores to Use (Beta)	Solve Process Settings
Adaptive Mesh Refinement	
Max Refinement Loops	1.

Refinement Depth	2.
Information	
Status	Done
MAPDL Elapsed Time	1 h 0 m
MAPDL Memory Used	12.118 GB
MAPDL Result File Size	7.4841 GB
Post Processing	
Distributed Post Processing (Beta)	Program Controlled
Mesh Source (Beta)	Program Controlled
Beam Section Results	No

Table 17

Model (A4) > Transient (A5) > Solution (A6) > Solution Information

Object Name	*Solution Information*
State	Solved
Solution Information	
Solution Output	Force Convergence
Newton-Raphson Residuals	0
Identify Element Violations	0
Update Interval	2.5 s
Display Points	All
FE Connection Visibility	
Activate Visibility	Yes
Display	All FE Connectors
Draw Connections Attached To	All Nodes
Line Color	Connection Type
Visible on Results	No
Line Thickness	Single
Display Type	Lines

Figure 63

Model (A4) > Transient (A5) > Solution (A6) > Solution Information

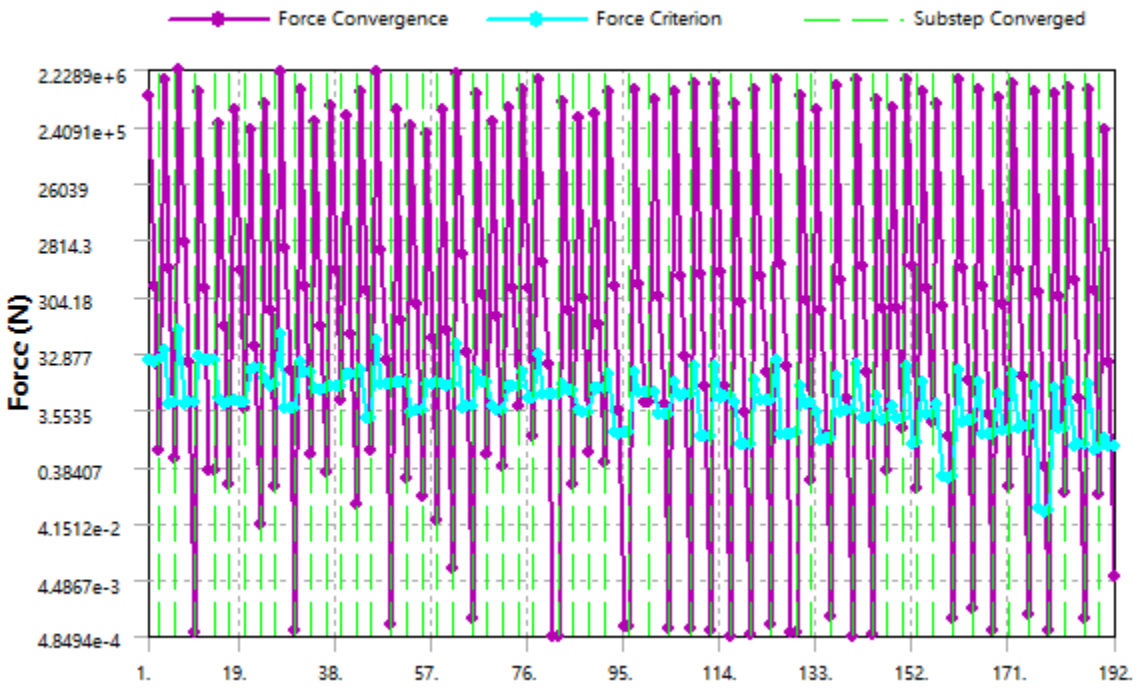

Figure 64

Model (A4) > Transient (A5) > Solution (A6) > Solution Information

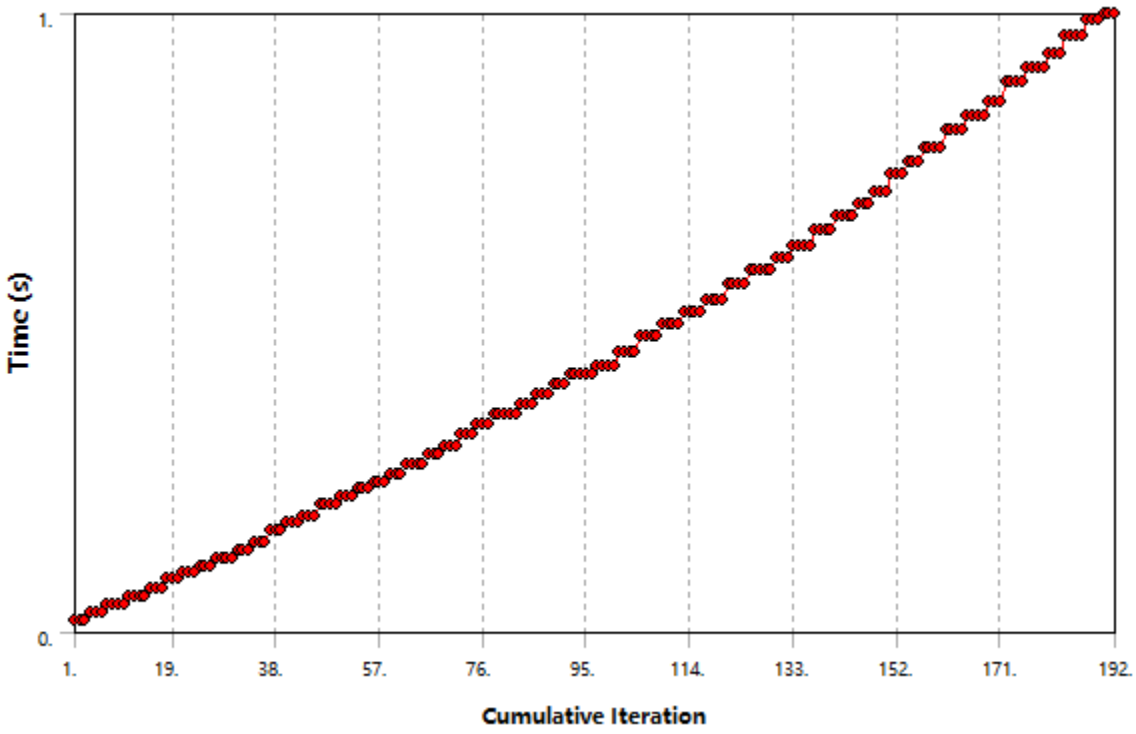

Table 18

Model (A4) > Transient (A5) > Solution (A6) > Results

Object Name	*Total Deformation*
State	Solved
Scope	
Scoping Method	Geometry Selection
Geometry	All Bodies
Definition	
Type	Total Deformation
By	Time
Display Time	Last
Calculate Time History	Yes
Identifier	
Suppressed	No
Results	

Minimum	278.7 mm
Maximum	429.78 mm
Average	357.73 mm
Minimum Occurs On	fall17-3 - Copy-63
Maximum Occurs On	fall17-3 - Copy-43
Minimum Value Over Time	
Minimum	2.1164 mm
Maximum	278.7 mm
Maximum Value Over Time	
Minimum	8.1237 mm
Maximum	429.78 mm
Information	
Time	1. s
Load Step	1
Substep	55
Iteration Number	192

Table 19

Model (A4) > Transient (A5) > Solution (A6) > Total Deformation

Time [s]	Minimum [mm]	Maximum [mm]	Average [mm]
2.e-002	2.1164	8.1237	4.6278
3.345e-002	7.4396	16.38	11.76
4.69e-002	12.751	27.478	20.394
5.8621e-002	16.474	35.542	26.394
7.0342e-002	19.098	38.864	29.38
8.7683e-002	21.361	43.02	32.251
9.7293e-002	23.127	47.245	35.063
0.1069	26.81	52.591	39.859
0.12132	32.979	63.338	48.718
0.13411	36.704	72.175	55.142
0.14691	39.933	75.749	58.484
0.16611	42.575	81.027	62.088
0.17739	45.317	86.135	66.051

0.18868	50.434	92.773	72.239
0.20561	56.142	105.06	81.548
0.21932	59.836	110.72	86.246
0.23303	62.45	113.33	88.661
0.24415	63.761	117.37	91.157
0.25526	67.361	122.8	95.782
0.27194	74.146	133.43	104.9
0.28647	78.388	141.98	111.44
0.301	82.04	145.45	114.91
0.31996	84.919	151.86	119.3
0.33648	90.689	159.9	126.41
0.353	96.653	170.4	134.97
0.36945	101.21	177.61	140.92
0.38591	104.54	181.71	144.44
0.4011	107.69	187.71	148.94
0.4163	113.79	195.33	156.08
0.43149	118.49	204.67	163.32
0.45208	124.01	211.63	169.54
0.47756	129.25	220.65	176.49
0.4975	136.49	229.97	185.04
0.51744	142.46	240.69	193.6
0.5376	147.83	246.87	199.31
0.5631	153.58	256.68	207.01
0.58599	161.49	267.6	216.71
0.60469	166.86	276.18	223.81
0.6234	171.49	281.95	228.92
0.64941	178.33	292.27	237.53
0.67297	186.02	303.37	247.18
0.69286	191.6	311.06	253.86
0.71276	196.31	317.8	259.51
0.74098	204.9	329.34	269.73
0.76182	211.12	338.8	277.74
0.78266	216.85	345.86	284.12
0.81391	225.1	357.81	294.26

0.83567	231.98	367.19	302.57
0.85744	238.15	375.56	309.91
0.88852	246.34	386.76	319.61
0.91154	253.47	395.92	327.88
0.93456	260.09	405.26	335.98
0.96326	267.87	415.43	344.97
0.98898	275.33	425.21	353.69
1.	278.7	429.78	357.73

Material Data

Structural Steel

Table 20

Structural Steel > Constants

Density	7.85e-009 tonne mm^-3
Isotropic Secant Coefficient of Thermal Expansion	1.2e-005 C^-1
Specific Heat Constant Pressure	4.34e+008 mJ tonne^-1 C^-1
Isotropic Thermal Conductivity	6.05e-002 W mm^-1 C^-1
Isotropic Resistivity	1.7e-004 ohm mm

Table 21

Structural Steel > Color

Red	Green	Blue
132	139	179

Table 22

Structural Steel > Compressive Ultimate Strength

Compressive Ultimate Strength MPa
0

Table 23

Structural Steel > Compressive Yield Strength

Compressive Yield Strength MPa
250

Table 24

Structural Steel > Tensile Yield Strength

Tensile Yield Strength MPa
250

Table 25

Structural Steel > Tensile Ultimate Strength

Tensile Ultimate Strength MPa
460

Table 26

Structural Steel > Isotropic Secant Coefficient of Thermal Expansion

Zero-Thermal-Strain Reference Temperature C
22

Table 27

Structural Steel > Alternating Stress Mean Stress

Alternating Stress MPa	Cycles	Mean Stress MPa
3999	10	0
2827	20	0
1896	50	0
1413	100	0
1069	200	0
441	2000	0
262	10000	0
214	20000	0
138	1.e+005	0
114	2.e+005	0
86.2	1.e+006	0

Table 28

Structural Steel > Strain-Life Parameters

Strength Coefficient MPa	Strength Exponent	Ductility Coefficient	Ductility Exponent	Cyclic Strength Coefficient MPa	Cyclic Strain Hardening Exponent
920	-0.106	0.213	-0.47	1000	0.2

Table 29

Structural Steel > Isotropic Elasticity

Temperature C	Young's Modulus MPa	Poisson's Ratio	Bulk Modulus MPa	Shear Modulus MPa
	2.e+005	0.3	1.6667e+005	76923

Table 30

Structural Steel > Isotropic Relative Permeability

Relative Permeability
10000